ORIGINAL ARTICLE

Relationships between ground motion parameters and energy demands for regular low-rise RC frame buildings

Emrah Meral[1] (ORCID)

Abstract

The present study aims to analyze the correlation between ground motion parameters and energy demands of low-rise RC buildings without shear walls. Two regular 4- and 7-story residential buildings were seismically designed to represent low-rise RC buildings. In order to establish the requirements of single degree of freedom (SDOF) systems as well as multi degree of freedom (MDOF) systems, the dynamic features of "equivalent" SDOF systems were defined by using MDOF systems. The correlation of 20 ground motion parameters (GMPs) of 44 records with the energy demands obtained from a total of 176 nonlinear time history analyses was examined for the SDOF and MDOF systems within the scope of this study. The ground motion parameters (GMPs) were taken as intensity measures (IMs). In contrast, maximum input energy was used as a demand measure (DM) and these energy values were normalized with the masses of the buildings for cases, where the buildings were evaluated together. Parameters related to acceleration and velocity are generally found to yield better results in comparison to the ones related to frequency and displacement. Velocity Spectrum Intensity (VSI) and Arias Intensity (I_a) were obtained to have the highest correlation values as a single parameter. This study suggested new equations by combining multiple ground motion parameters for SDOF and MDOF systems to better reflect damage potential than a single parameter. The use of multiple parameters in combination results in better correlation coefficients.

Keywords Ground motion parameters · Seismic intensity measures · Low-rise RC frame buildings · Nonlinear time history analysis · Input energy

List of symbols

AIDR	Average interstory drift
ASI	Acceleration spectrum intensity
A95	Ground motion parameter that changes depending on arias intensity
A_{rms}	RMS of acceleration
A_{max}/V_{max}	Ratio of peak acceleration to peak velocity
CAV	Cumulative absolute velocity
CP	Collapse prevention

✉ Emrah Meral
emrahmeral@osmaniye.edu.tr

1 Department of Civil Engineering, Osmaniye Korkut Ata University, 80000 Osmaniye, Turkey

CSA	Characteristic spectral acceleration
DD-1	Maximum earthquake level
DD-2	Design earthquake level
DM	Demand measure
D_{rms}	RMS of displacement
EDA	Effective design acceleration
EPA	Effective peak acceleration
E_A	Total energy
E_D	Damping energy
E_H	Hysteretic energy
E_I	Input energy
E_K	Kinetic energy
E_S	Elastic strain energy
GMP	Ground motion parameter
HI	Housner intensity
IM	Intensity measure
IO	Immediate occupancy
I_a	Arias intensity
I_c	Characteristic intensity
LS	Life safety
MDOF	Multi degree of freedom
MIDR	Maximum interstory drift ratio
OSDI	Overall structural damage index
PEER	Pacific Earthquake Engineering Research
PGA	Peak ground acceleration
PGD	Peak ground displacement
PGV	Peak ground velocity
PSV	Pseudo spectral velocity
RMS	Root-mean-square
RSA	Representative spectral acceleration
S_a	Spectral acceleration
SA	Spectral pseudo-acceleration
SDOF	Single degree of freedom
SED	Specific energy density
SMA	Sustained maximum acceleration
SMV	Sustained maximum velocity
SRSS	Square root of the sum of squares
TBEC 2018	2018 Turkish Building Earthquake Code
t_e	Effective duration
T_m	Mean period
T_p	Predominant period
V_{rms}	RMS of velocity
VSI	Velocity spectrum intensity
V_{s30}	Shear wave velocity

Symbols

ξ	Damping ratio
ε_{co}	Unconfined concrete compressive strain

ε_{cc}	Confined concrete compressive strain
ε_{cu}	Maximum compressive strain of confined concrete
ε_{sy}	Yield strain of the reinforcement steel
ε_{sh}	Strain in steel at the onset of strain hardening
f_{cc}	Confined concrete strength
f_{co}	Unconfined concrete strength
f_{sy}	Yield strength of reinforcement steel
f_{su}	Maximum strength capacity of steel

1 Introduction

It is essential to estimate the earthquake damage for the seismic performance of new buildings and the evaluation of existing structures by considering the potential future earthquake hazard. Assessment of ground motion intensity measure (IM) and demand measure (DM) together allows for the prediction of the damage risk of the earthquake. The ground motion parameters (GMPs) such as peak ground acceleration (PGA) and velocity (PGV), etc. have been taken as intensity measures (IMs), whereas the structural damage is quantified by demand measures (DMs) such as maximum roof drift ratio and input energy, etc. (Akkar and Özen 2005). The GMPs showing a good correlation with DMs indicate that the seismic performances of the structures are obtained properly. Therefore, examinations of the GMP that best reflects the seismic damage potential statistically are still conducted today.

There are many studies showing an interdependency between the behavior of structures and GMPs. Elenas (2000) emphasized that Park/Ang and DiPasquale/Çakmak as damage index had a high correlation with spectral pseudo-acceleration (SA), medium correlation to PGV, peak ground displacement (PGD) and I_a, whereas they had a poor to medium correlation to effective peak acceleration (EPA) and a poor correlation with PGA and the ratio of peak acceleration to peak velocity (A_{max}/V_{max}). Elenas and Meskouris (2001) took into account demand measures (DMs) such as the overall structural damage index (OSDI), maximum interstory drift ratio (MIDR), and maximum floor acceleration. The authors reported that SA had a strong correlation with OSDI and MIDR, while PGA had a poor correlation. I_a showed a high correlation, whereas A_{max}/V_{max} had a low correlation with max. floor acceleration.

Akkar and Özen (2005) stated that the PGV had a higher correlation with spectral displacements on SDOF systems for short periods when compared to PGA and PGV/PGA. PGV also showed a more consistent correlation with inelastic displacement demands according to spectral acceleration (S_a). Yakut and Yilmaz (2008) concluded that Housner intensity (HI), velocity spectrum intensity (VSI), and acceleration spectrum intensity (ASI) had the strongest correlation with maximum interstory drift ratio (MIDR) for structures with the period range of 0.1–2.5 s. PGA, VSI, and characteristic intensity (I_c) were the parameters with the highest correlation for periods between 0.2–0.5 s, while VSI, HI, and S_a were found to be the best parameters for periods between 0.5 and 1.1 s.

Cao and Ronagh (2014) investigated the relation between maximum interstory drifts, Park/Ang damage index, and the characteristics of 1040 far-fault ground motion records. They indicated that PGD, PGV/PGA, displacement rms (D_{rms}), specific energy density (SED), predominant period (T_p), and mean period (T_m) had poor correlations with the damage of structures. VSI was the best parameter of seismic damage potential, followed by HI and S_a. The findings also revealed that PGA had a weak correlation with

structural damage when compared to other parameters. The overall structural damage index, as well as the maximum (MIDR) and average interstory drift (AIDR) as structural damage states, was correlated with GMPs by Kostinakis et al. (2015). Given the results, S_a, followed by VSI, PGV, and HI, correlated well with MIDR or AIDR as the indicator of structural damage, whereas PGV/PGA and D_{rms} were GMPs with the least influence. Furthermore, the overall structural damage index showed a moderate to low correlation with most of the GMPs.

The correlation between nonlinear displacement drift demands and ground motion features was examined using the number of story and soil classes by Ozmen and Inel (2016). PGA and PGD were found to have a poor correlation with damage in comparison to the VSI, PGV, and several different parameters such as effective design acceleration (EDA) and I_c. The effect of GMPs on structural damage, which includes inter-story drift, roof drift, and the Park/Ang index, was examined using regression coefficients by Massumi and Gholami (2016). They emphasized that VSI had the highest effect, followed by the HI.

The damage potential of ground motion records was investigated by using correlation coefficients between GMPs and displacement demands obtained from SDOF models and MDOF buildings that have diverse lateral strength capacities and periods depending on different soil properties by Palanci and Senel (2019). The correlations of PGA, PGV, and spectrum intensity (SI) are generally better than others, while PGA, root mean square (RMS) of acceleration (A_{rms}), and ASI have good correlations at short vibration periods of structures. In addition, correlation coefficients acquired from MDOF buildings are quite similar to the results of SDOF models. Kamal and Inel (2021) studied the correlation of GMPs with inelastic roof drift ratios of mid-rise RC frame buildings taking into account soil-structure interaction. HI has a higher correlation than all parameters while root mean square (RMS) of velocity (V_{rms}), VSI, SED, sustained maximum velocity (SMV), and PGV have a good correlation. The lowest correlations were found with the PGA and A95 parameters. The relationship between spectral acceleration and response measures (interstory drift, local deformation demand, and dissipated energy) was examined for both bare and infilled regular moment frames by Papasotiriou et al. (2022). The authors emphasized that spectral acceleration can be considered an effective parameter reflecting the damage of moment frames. The correlation between 31 GMPs, including the proposed characteristic spectral acceleration (CSA) and representative spectral acceleration (RSA) parameters, and structural damage (top displacement, interstory drift, and column ductility demand) was examined on 1568 bare and infilled low-rise frame sets by Papasotiriou and Athanatopoulou (2022). Among those parameters, RSA and CSA were found to have the highest correlation with damage.

There are few studies that have examined the relationship between GMPs and energy demand parameters as an indicator of structural damage. Riddell and Garcia (2001) carried out a study in order to define GMPs that correlated well with input (E_I) and hysteretic (E_H) energy in SDOF systems. They concluded that peak ground motion parameters (PGA, PGV, and PGD) showed a good correlation with energy dissipation in the long (displacement region) and short (acceleration region) period for response spectra, whereas HI is the best parameter in the medium period (velocity region). Riddell (2007) examined the correlation between 23 ground motion intensity indices with four response variables such as elastic-inelastic deformation demands and input-hysteretic energy for SDOF systems. Even though PGA and PGD exhibited a better correlation with input and hysteretic energies in relation to spectral regions, PGV had a moderate correlation. HI was the best parameter in the velocity region depending on correlation with both displacement and energy demands,

while it has a poor and moderate correlation in the acceleration and displacement regions, respectively. In the short period range, I_a shows a good correlation with energy demands.

Yang et al. (2009) conducted a correlation analysis between 30 intensity measures (IMs) parameters and three demand measures (DMs) (maximum inelastic displacement, input, and hysteretic energy) of SDOF systems. The acceleration-related parameters (I_c and I_a) are highly correlated with demand variables in the short period range. The velocity-related parameter (PGV) exhibits a good correlation in the medium and long period ranges. Koç (2017) examined the effects of ground motion characteristics and structural features on the distribution of seismic input energy depending on the MDOF system using various types of ground motion records. Given the analysis results, a very high correlation is determined between the input energy (E_I) and the pseudo-spectral velocity (PSV). Merter (2019) indicated that there is a good relationship between the maximum input energy demands of linear time history analysis and the approach he proposed for SDOF systems. The suggested equation including PSV_{max} and I_a correctly estimates the maximum elastic input energy.

In line with the studies in the literature, it was planned to carry out a study with distinctive characteristics. Examining the previous studies mentioned above, it can be seen that it is difficult to achieve a definitive conclusion about the intensity of GMPs that represent the damage estimation of MDOF and SDOF systems. Most of these studies focused on different damage indexes, maximum interstory, and roof drifts as damage indicators. On the other hand, there are few studies, in which damage was associated with energy. Although previous studies were generally carried out on the SDOF system, ones related to the MDOF system are usually based on a single structure or a two-dimensional (2D) frame building. In addition, either ground motion records or GMPs are considered in very few studies. The present study examined the correlation of GMPs with input energy demands of low-rise RC buildings. It was scaled by selecting 44 real earthquake records in compliance with the Turkish Building Earthquake Code (TBEC 2018). Twenty GMPs based on 10 different seismic events were considered for each selected record. Maximum input energy was used as demand measurement and energy demands were normalized by the mass of the buildings. The relationship between roof displacements and input energy was also examined for the considered buildings. Moreover, the distribution of hysteretic energy to floors and structural elements was also examined in this study.

2 Ground motion parameters

Summary definitions of the ground motion parameters examined here are provided in this section. More detailed information can be found in the book "Geotechnical Earthquake Engineering" by Kramer (1996). SeismoSignal (2022) software was used in order to obtain the values of the parameters in this study. A total of 20 ground motion parameters (GMPs), which are used to examine the correlation between the parameters and the energy demands for SDOF and MDOF systems, are described mainly considering the content and the peak values of the ground motion records below:

- *Peak Ground Acceleration (PGA):* PGA is the simplest ground motion parameter that is widely used to define the severity of an earthquake. Indicators of seismic excitations cannot be described by the PGA alone (Elenas 1997) (Eq. 1).

$$PGA = \max |a(t)| \tag{1}$$

- *Peak Ground Velocity (PGV):* Akkar and Özen (2005) demonstrated that PGV correlated better with SDOF deformation demands obtained from analyses when compared to other ground motion intensity measures (Eq. 2).

$$PGV = \max |v(t)| \tag{2}$$

- *Peak Ground Displacement (PGD):* Elenas (2000) and Elenas and Meskouris (2001) used this parameter to examine the correlation with the structural damage (Eq. 3).

$$PGD = \max |d(t)| \tag{3}$$

In the equations, a(t), v(t), and d(t) refer to the acceleration, velocity, and displacement history.

V_{max}/A_{max}: This V_{max}/A_{max} ratio has been utilized for near-field ground motions by researchers (Liao et al. 2001; Sucuoğlu et al. 1998; Sucuoğlu and Nurtuğ 1995; Zhu et al. 1988). (Eq. 4)

$$PGV/PGA = \frac{\max |v(t)|}{\max |a(t)|} \tag{4}$$

- *Root-mean-square (RMS) of acceleration, velocity, and displacement:* These parameters are calculated by Eqs. (5)–(7) where t_t is the total duration of the ground motion record.

$$a_{RMS} = \left[\frac{1}{t_t} \int_0^{t_t} [a(t)]^2 dt \right]^{1/2} \tag{5}$$

$$v_{RMS} = \left[\frac{1}{t_t} \int_0^{t_t} [v(t)]^2 dt \right]^{1/2} \tag{6}$$

$$d_{RMS} = \left[\frac{1}{t_t} \int_0^{t_t} [d(t)]^2 dt \right]^{1/2} \tag{7}$$

- *Arias Intensity (I_a):* I_a was proposed by Arias (1970) as a ground motion parameter related to the energy content of the ground motion and is presented in Eq. (8). Some researchers emphasized that I_a has a good correlation with demand measures of structural performance, liquefaction, and seismic slope stability (Travasarou et al. 2003).

$$I_a = \frac{\pi}{2g} \int_0^{t_t} \left[a(t)^2 \right] dt \tag{8}$$

- *Characteristic Intensity (I_c):* The characteristic intensity (I_c) includes both the acceleration (see Eq. 5) and duration-related parameters. It is expressed by Eq. (9).

$$I_c = \left(a_{RMS} \right)^{3/2} \sqrt{t_t} \tag{9}$$

- *Cumulative Absolute Velocity (CAV):* This parameter is defined with Eq. (10) as the area under the absolute accelerogram. CAV was discovered by Reed et al. (1988) in a study, which was sponsored by the Electric Power Research Institute. Cabañas et al. (1997) determined that CAV has a good correlation with damage.

$$CAV = \int_0^{t_t} |a(t)|dt \tag{10}$$

- *A95 parameter:* The acceleration level down, which 95 percent of the I_a is contained. This parameter was defined by Sarma and Yang (1987) and it can be calculated by using Eq. (11).

$$A95 = 0.764 I_a^{0.438} \tag{11}$$

- *Acceleration (ASI) and Velocity (VSI) Spectrum Intensity:* ASI and VSI are calculated via spectral acceleration and velocity, respectively by Von Thun et al. (1988) in Eqs. (12, 13), where ξ refers to the damping ratio. S_a and S_v refer to acceleration and velocity spectrum, respectively.

$$ASI = \int_{0.1}^{0.5} S_a(T)dT \, (\xi = 0.05) \tag{12}$$

$$VSI = \int_{0.1}^{2.5} S_v(T)dT \, (\xi = 0.05) \tag{13}$$

- *Housner Intensity (HI):* This parameter was suggested by Housner (1952) and is given in Eq. (14). The VSI and HI are similar parameters, the only difference is that VSI is calculated from the absolute velocity spectrum, whereas HI is based on the pseudo velocity spectrum.

$$HI = \int_{0.1}^{2.5} PSV(T)dT \, (\xi = 0.05) \tag{14}$$

- *Specific Energy Density (SED):* SED is determined by Eq. (15).

$$SED = \int_0^{t_t} [v(t)]^2 dt \tag{15}$$

- *Sustained Maximum Acceleration (SMA) and Velocity (SMV):* SMA and SMV are identified as the third-highest absolute value of acceleration and velocity in the time history as proposed by Nuttli (Nuttli 1979).
- *Effective Design Acceleration (EDA):* EDA corresponds to the peak acceleration value found after lowpass filtering the input time history with a cut-off frequency of 9 Hz (Reed et al. 1988).

- *Predominant Period (T_p):* T_p is the period, at which the maximum spectral acceleration occurs in an acceleration response spectrum computed at 5% damping level.
- *Mean Period (T_m):* T_m is the best simplified frequency content characterization parameter, which is estimated using Eq. (16), where C_i are the Fourier amplitudes, and f_i represent the discrete Fourier transform frequencies between 0.25 and 20 Hz (Rathje et al. 1998).

$$T_m = \frac{\sum C_i^2 / f_i}{\sum C_i^2} \tag{16}$$

Many parameters have been recommended to estimate the damage potential of strong ground motions. Some of these parameters are obtained from the ground motion records or the response spectra, while other parameters are calculated using the equations. Ground motion parameters are divided into four classes: acceleration-related, velocity-related, frequency-related, and displacement-related. The parameters and their abbreviations used in the present study are listed in Table 1.

Table 1 Definitions of the ground motion parameters

Type	Parameter	Identifier	Unit
Acceleration	Arias intensity	I_a	m/s
	Characteristic Intensity	I_c	–
	Root mean square (RMS) of acceleration	A_{rms}	g
	Sustained maximum acceleration	SMA	g
	Acceleration spectrum intensity	ASI	g.s
	Peak ground acceleration	PGA	g
	Effective design acceleration	EDA	g
	A95 parameter	A95	g
Velocity	Velocity spectrum intensity	VSI	m
	Housner intensity	HI	m
	Cumulative absolute velocity	CAV	m/s
	Sustained maximum velocity	SMV	m/s
	Peak ground velocity	PGV	m/s
	Root mean square (RMS) of velocity	V_{rms}	m/s
	Specific energy density	SED	m²/s
Frequency	Predominant period	T_p	s
	Ratio of peak velocity to peak acceleration	V_{max}/A_{max}	s
	Mean period	T_m	s
Disp.	Peak ground displacement	PGD	m
	Root mean square (RMS) of displacement	D_{rms}	m

3 Prototype low-rise RC frame buildings

3.1 Buildings description

Two sets of 4- and 7-story building models were designed to represent the low-rise buildings that constitute most of the current RC building stock in Turkey. The models were created as residential buildings in compliance with the 2018 Turkish Building Earthquake Code (TBEC 2018). The structural system of buildings consists of frames with beams and columns but no shear walls. Since building models were designed as residential buildings, the building importance coefficient (I) of relevant structures was assumed to be 1 in compliance with the TBEC (2018). Since seismic loads are carried by moment frames with high ductility levels, structural system behavior factor (R) was accepted as 8 per relevant regulation. The buildings considered here have the same mold plan as shown in Fig. 1. The plans of 3D buildings were symmetrical in both X and Y directions. The building models had no irregularity in plan and elevation. The heights of all floors were assumed to be 2.8 m along the building elevation. The beam dimensions were considered to be 250×500 mm and 250×600 mm for 4- and 7-story buildings, respectively. The column dimensions were selected as 400×400 mm and 500×500 mm for 4- and 7-story buildings, respectively.

The typical steel stress–strain model with strain-hardening and the unconfined and confined concrete models proposed by Mander et al. (1988) were applied to RC beam and column sections. When the expected concrete strength (f_{co}) is taken as 25 MPa for unconfined concrete, the concrete compressive strain (ε_{co}) corresponding to this value is 0.002. While confined concrete strength (f_{cc}) increases to 31.35 MPa due to the coating, the concrete
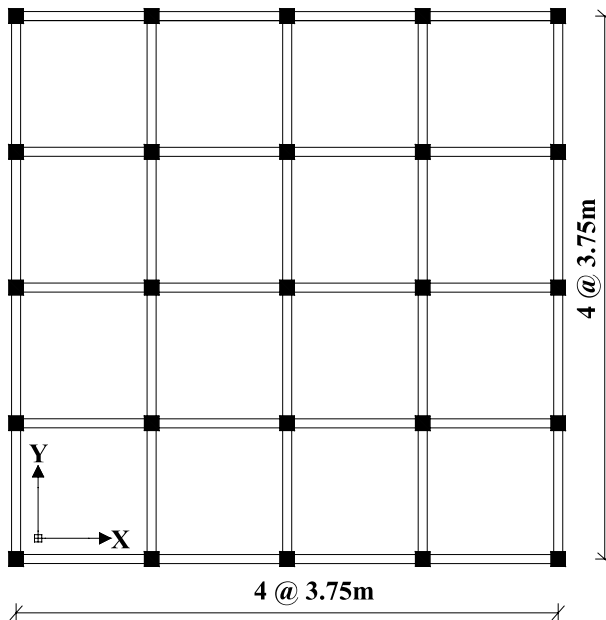

Fig. 1 Plan layout of MDOF buildings

compressive strain (ε_{cc}) then becomes 0.004. In addition to these deformation values, the maximum compressive strain (ε_{cu}) in confined concrete is 0.0174. The yield strength (f_{sy}) of both longitudinal and transverse reinforcement was assumed to be 420 MPa for the present study. As the elasticity modulus (E_s) of steel was taken as 200,000 MPa, the yield strain (ε_{sy}) of the steel was calculated to be 0.0021, and the strain (ε_{sh}) in steel was considered to be 0.01 at the onset of strain hardening. When the steel reaches maximum strength capacity (f_{su}) as 500 MPa, the maximum strain capacity (ε_{su}) of the steel becomes 0.09. The tensile-deformation relationships defined for concrete and steel are presented in Fig. 2. The longitudinal reinforcement ratios of the columns were taken as approximately 1% for both 4- and 7-story buildings. Peripheral stirrups are used as transverse reinforcements at 100 mm spacing to reflect the ductile detailing compatible with the regulation. In addition to the peripheral stirrups, one crosstie with the same spacing as stirrups was considered in both directions for the column elements.

The slab thickness was taken as 150 mm in all floors of 4- and 7-story building models. Since the load-carrying system of the buildings consists of frames with beam and column members, slabs are not created as structural elements during the design stage. The weight of the slabs is transferred together with the coatings and other loads on them to the beams around these slabs. It is assumed that there is an infill wall load of 4.5 kN/m on the other beams, except for the beams on the roof floor. The vertical loads other than the wall weight were considered as a dead load (g) of 3.75 kN/m^2 and a live load (q) of 2.0 kN/m^2 (1.5 kN/

Fig. 2 Stress–strain plots: **a** strength-strain relations for unconfined and confined concrete, **b** strength-strain relationship for reinforcement steel
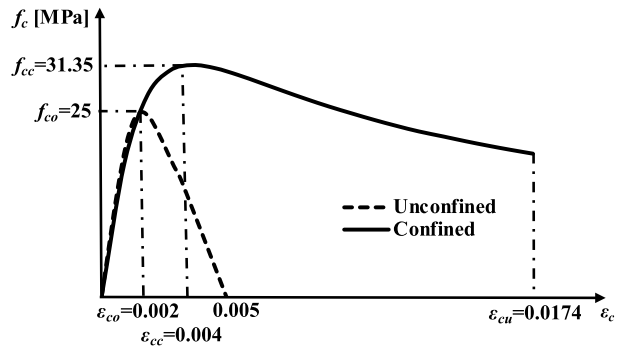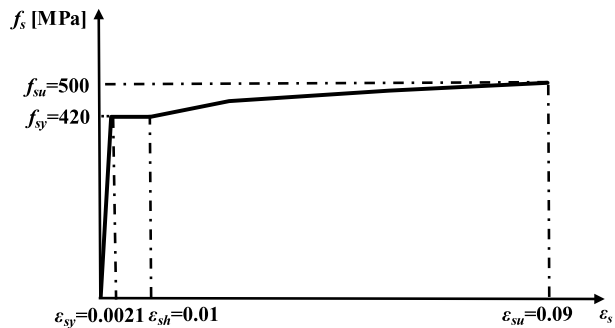
m^2 on upper floor) on the floors. The contribution to the lateral strength of infill walls is disregarded in building models in the present study. Rigid diaphragms were applied separately at each floor level in order to transfer earthquake loads to the carrier elements in proportion to their stiffness. It should be noted that the mass of the structures was calculated by proportioning the weight values corresponding to the sum of the dead loads (g) and 30% of the live loads (q) to the gravitational acceleration.

The inelastic dynamic characteristics of MDOF buildings were converted into values of "equivalent" SDOF systems in order to analyze SDOF models. For this purpose, the capacity curves reflecting the horizontal load-carrying capacity of the buildings were obtained from the pushover analysis of the building models. Modal load pattern was used as horizontal load distribution in pushover analyses. The base shear was normalized by building weight, while the roof displacement was normalized by building elevation to represent the shear strength coefficient and roof drift ratio, respectively. The capacity curves were approximated with a bilinear curve in accordance with the principles specified in the FEMA-356 (2000) guideline. Capacity curves of considered buildings are given in Fig. 3.
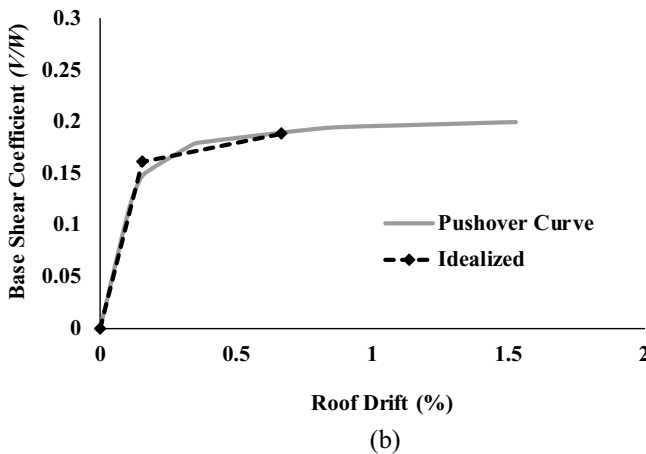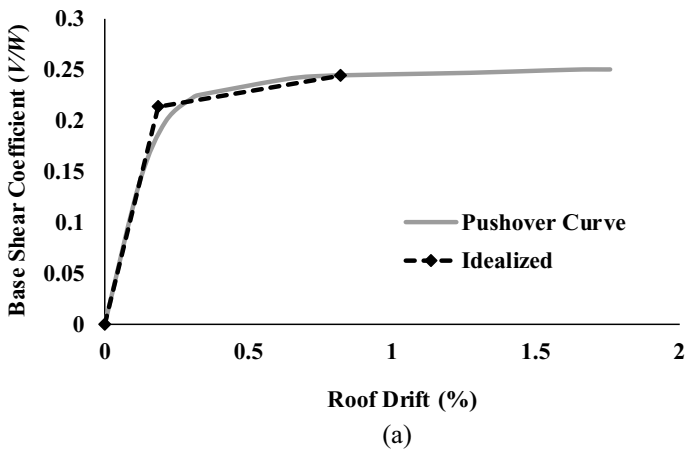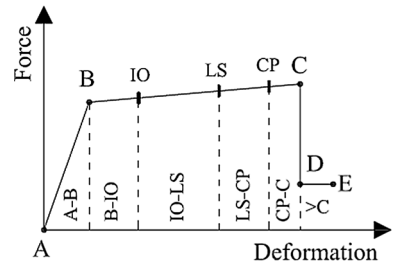

Fig. 3 Capacity curves: **a** for 4-story and **b** for 7-story building models

Table 2 Structural features of building models

Building models	Period (s)	Effective participating mass ratios (%)	Seismic mass (kNs²/m)	V_y/W (%)	Post-yield stiffness ratios
4-story	0.50	82.4	985.09	0.21	0.042
7-story	0.67	81.6	1953.56	0.16	0.051

Fig. 4 Typical force–deformation relation for an auto-plastic hinge

Strength ratios at yield point (V_y/W) and post-yield stiffness ratios (plastic/elastic stiffness ratios) were calculated by using the idealized capacity curves (bilinear curves). The parameters reflecting the dynamic behavior of the structures are shown in Table 2. Structural response information such as dominant vibration periods and effective participating mass ratios depends on the results of modal analysis. Moreover, since the effective participating mass ratio of the first (dominant) vibration mode must be at least 0.70 in order to use pushover analysis in accordance with the TBEC (2018), it can be seen in Table 2 that this condition is met.

3.2 Structural modeling

SAP2000 (2018), which is a general-purpose structural analysis program, was used in modeling and nonlinear analyses of structures. Beams and columns were modeled as nonlinear stick members by using lumped plastic behavior model by defining plastic hinges at both ends of beams and columns. The length of the plastic deformation region was assumed to be equal to ½ of the section depth of structural members in accordance with TBEC (2018) and other regulations (e.g., ATC-40 (1996) and FEMA-356). SAP2000 enables definition options of plastic hinges such as user-defined hinge properties or auto (default) hinge properties explained in FEMA-356 and ASCE 41-13 (2014), which are used in the present study to assign the nonlinear behavior of frame elements. Automatic hinges require detailed information (material characteristics, dimensions of members, longitudinal and transverse reinforcement contents, etc.) of the frame section property used by structural elements. The five points such as A, B, C, D, and E that define the strength-displacement (as moment-rotation) relationship of a typical plastic hinge are shown in Fig. 4. The immediate occupancy (IO), life safety (LS), and collapse prevention (CP) are described as performance levels in FEMA-356 and ASCE 41-13. Bending rigidity of the beams and columns was multiplied by stiffness modification factors as 0.35 and 0.70 explained in TBEC (2018) to regard the effective stiffness of the cracked section, respectively.

The direct integration method between two solution options as modal and direct integration was chosen for time history analysis of MDOF building models. A variety of widely used methods such as Chung and Hulbert, Collocation, Hilber-Hughes-Taylor, Wilson and Newmark are available for performing time history analysis with direct integration. The Newmark method with gamma (γ)=0.5 and beta (β)=0.25 was applied for nonlinear time history analyses in this study. Mass and stiffness proportional coefficients were specified using the 5% damping rate by different periods for viscous proportional damping.

4 Selected ground motion records

For more reliable results, the real ground motion records are used in nonlinear time history analyses. These records include precise data such as amplitude, frequency, and duration of seismic events. They also reflect factors like soil properties and source distance that affect records. Because of these reasons, the selection and scaling of real records are very important in order to determine accurately the effects to be examined.

Two different reinforced concrete buildings representing low-rise structures were assumed to be located on the soil class ZD defined in TBEC (2018) near Osmaniye Korkut Ata University in Osmaniye province of Turkey. The design (DD-2) and maximum (DD-1) earthquake levels, in which 10 and 2% probability of exceedance in 50 years, respectively, were considered while selecting the records. Two target response spectra were obtained to reflect the regional earthquake hazard by considering the coordinates of buildings, soil type, and different earthquake levels. The parameters that control the shape of considered spectra are given in Table 3. In Table 3, the corner periods of the horizontal elastic acceleration spectra are described as T_A and T_B. Spectral acceleration coefficients for short and 1.0 s periods are expressed as S_{DS} and S_{D1}, respectively. A total of 22 ground motion record sets from 10 different earthquakes compatible with target spectra were taken from the PEER (Pacific Earthquake Engineering Research) ground motion database (PEER 2019). Acceleration records in accordance with design and maximum acceleration spectra principles of TBEC (2018) were scaled by using simple scaling method for spectral matching between target spectra and spectrum of selected records via PEER. The horizontal spectrum was generated by taking the square root of the sum of squares (SRSS) of the spectra of the scaled horizontal components belonging to each earthquake record pair. Ground motion components are scaled according to the rule that the average of the resultant spectra of the records should not be less than 1.3 times the target spectra in the period intervals specified in TBEC (2018). Resultant spectra related to 22 ground motion record sets, mean of resultant spectra, and target spectra curve amplified with 1.3 coefficient for design (DD-2) and maximum (DD-1) earthquake levels are given in Fig. 5. Although the resultant spectra of selected records for especially periods of considered building models have spectral acceleration values in a wide band range, it can be seen in Fig. 5 that average of these spectra is quite compatible with the 1.3 times target spectra. In other words, it can be said that the average of the resultant spectra of the selected records ensures the requirement of being 1.3 times the regulation spectrum. The features of the selected records and their

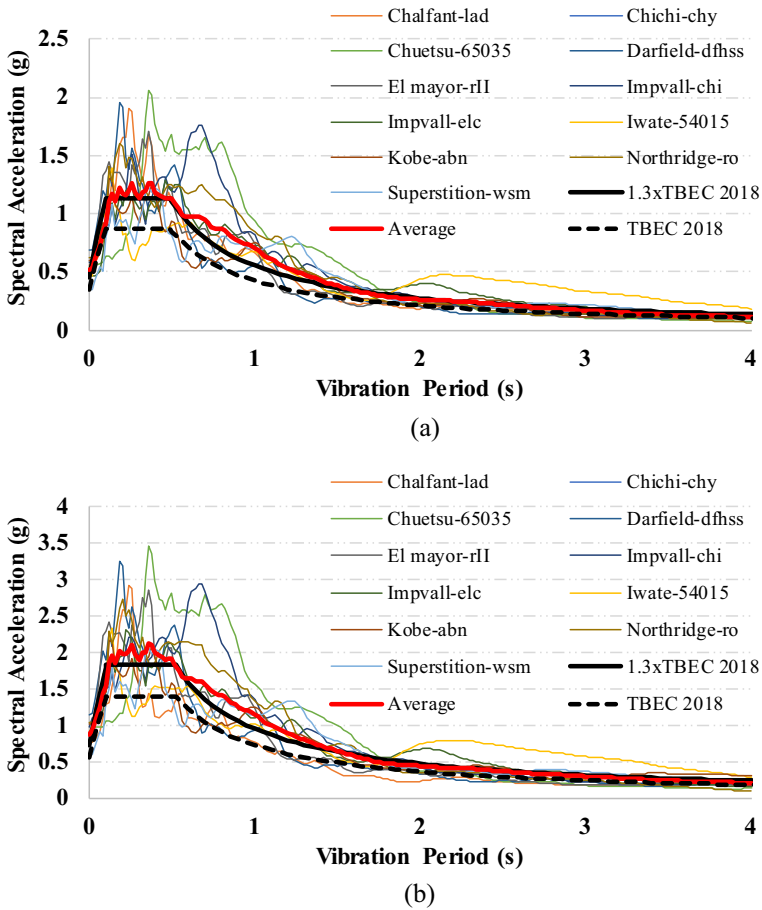| Table 3 Parameters of elastic acceleration spectra for the selected location of buildings	Seismic level	T_A (s)	T_B (s)	S_{DS}	S_{D1}
	DD-2	0.097	0.487	0.873	0.425
	DD-1	0.104	0.520	1.405	0.731

Fig. 5 The resultant spectra of scaled earthquake record sets for 5% damping: **a** for DD-2 and **b** for DD-1 earthquake levels

scale factors are seen in Table 4. Although the earthquake magnitudes (M_w) changed between 6.2 and 7.2, the distances were limited between 5 and 25 km. The shear wave velocity (V_{s30}) was chosen between 180 and 360 m/s to reflect the ZD soil class per TBEC (2018). Scaling coefficients sensibly range between 0.84 and 1.89 and between 1.40 and 3.16 for design (DD-2) and maximum (DD-1) earthquake levels, respectively. Both horizontal components were scaled with the same scaling factors. Number of earthquake record sets should be at least 11 and number of record pairs to be selected from the same earthquake shall not exceed three for time history analysis in accordance with TBEC (2018). The aforementioned circumstances in the regulation were taken into account in the selection and scaling of the ground motion records. In some studies, ground motions were also classified as pulse-like and non-pulse-like (Baker 2007; Zhai et al. 2013). Researchers specified that pulse-like ground motions create higher demands on structures than expected according to the response spectra.

Since the effective time of the ground motion increases, more energy input is expected for the structure. The most important difference of the energy parameters from other variables (base shear force and roof displacement etc.) is that they are not obtained as an instantaneous

Table 4 Characteristics of ground motion records used in the present study

No.	Earthquake	Record	Station	Scale Factor (DD-2)	Scale Factor (DD-1)	Date	Magnitude	V_{s30} (m/s)	Rjb (km)	$Rrup$ (km)	te (s)
1	Chalfant Valley	lad180	Bishop—LADWP South St	1.83	3.06	21.07.1986	6.2	303.47	6.09	6.09	17.18
2		lad270									
3	Chi–Chi	chy101e	Chy101	1.82	3.05	20.09.1999	6.2	258.89	7.29	7.29	18.44
4		chy101n									
5	Chuetsu	65035ew	Shiura Nagaoka	1.74	2.91	16.07.2007	6.8	336.93	14.38	17.17	25.85
6		65035 ns									
7	Darfield	dfhss17e	Dfhs	0.98	1.64	04.09.2010	7.0	344.02	13.03	13.03	21.75
8		dfhss73w									
9	El Mayor	rii000	RIIto	0.84	1.40	04.04.2010	7.2	242.05	5.59	10.05	26.24
10		rii090									
11	Imperial valley	chi012	Chihuahua	1.56	2.62	15.10.1979	6.5	242.05	24.85	24.85	24.26
12		chi282									
13	Imperial valley	elc180	El Centro Array #9	1.32	2.21	15.10.1979	6.5	213.44	21.62	21.67	24.20
14		elc270									
15	Iwate	54015ew	Iwadeyama	1.04	1.74	14.06.2008	6.9	345.55	10.61	20.17	15.45
16		54015 ns									
17	Kobe	abn000	Abeno	1.89	3.16	16.01.1995	6.9	256.00	20.77	20.78	56.39
18		abn090									
19	Northridge	ro3000	Sun Valley—Roscoe Blvd	1.19	1.99	17.01.1994	6.7	320.93	13.70	13.71	16.74
20		ro3090									
21	Superstition hills	wsm090	Westmorland Fire Sta	1.28	2.14	24.11.1987	6.5	193.67	11.86	11.86	23.52
22		wsm180									

$Rjb*$ is Joyner-Boore distance defined as the closest horizontal distance to rupture plane (as epicentral distance)

$Rrup*$ is the closest distance to the rupture plane

maximum value but they are calculated by summing the effects that occur during the ground motion. Many definitions such as "bracketed duration", "uniform duration" and "significant duration" which vary according to the measured value have been made in order to determine the effective duration of the earthquake (Fahjan 2008). The parameter used in the calculation of the significant duration, which shows the time it takes for the energy in the acceleration record to be discharged, is the Arias intensity (I_a), which indicates the amount of energy in the record. The curve showing the change of Arias Intensity (I_a) over time as a percentage is expressed as "Husid Plot". The time between 5% and 95% occurrence of Arias Intensity (I_a) over this curve is defined as "significant duration". The effective duration (t_e) of the records used in the study was determined with significant duration and added to Table 4. Figure 6 shows the effective duration for the Kobe-abn090 ground motion record. The effective duration of the record, which has a total recording time of 140 s, is calculated approximately as 56 s by the time difference ($t_2 - t_1$).

5 Energy-based design

5.1 Theoretical approach

Energy-based structural computation is a design method that investigates the distribution of the energy entering the building with strong ground motion to the structural elements and the consumption of this energy by the structural members. In order to address the energy phenomenon and energy-related parameters in building systems, the equation of motion of the SDOF system should be considered first. The seismic response of the SDOF system subjected to horizontal ground motion is expressed by the general dynamic equation of motion (Eq. 17).

$$m\ddot{u} + c\dot{u} + ku = -m\ddot{u}_g(t) \tag{17}$$

where m, c and k represent mass, damping and stiffness, respectively. $\ddot{u}$, $\dot{u}$, u, and $\ddot{u}_g$ are acceleration, velocity, displacement and acceleration of strong ground motion, respectively.
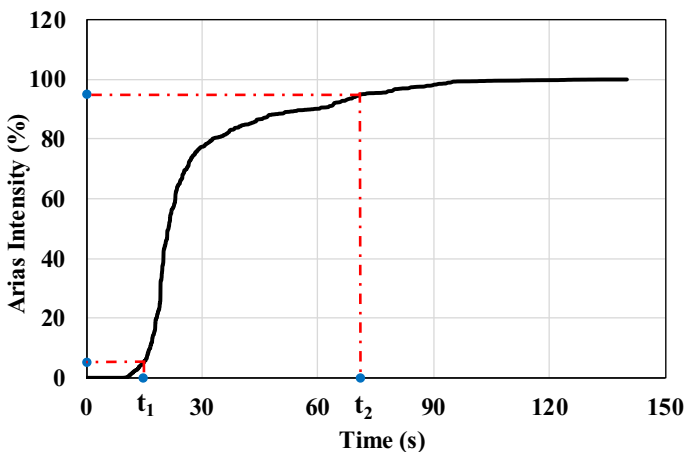

Fig. 6 Determination of significant duration for Kobe-abn090 record using Husid Plot

As a result of integrating Eq. (17) with respect to displacement, the general energy equation is obtained as Eq. (18).

$$\int_0^{u(t)} m\ddot{u}(t)du + \int_0^{u(t)} c\dot{u}(t)du + \int_0^{u(t)} ku(t)du = -\int_0^{u(t)} m\ddot{u}_g(t)du \qquad (18)$$

The energy equation is easily related to the duration of the ground motion by writing $du = \dot{u}\,dt$ in Eq. (18), and the integrals are expressed in terms of time as Eq. (19).

$$\int_0^{t} m\ddot{u}(t)\dot{u}dt + \int_0^{t} c\dot{u}(t)\dot{u}dt + \int_0^{t} ku(t)\dot{u}dt = -\int_0^{t} m\ddot{u}_g(t)\dot{u}dt \qquad (19)$$

The input energy (E_I) caused by the earthquake is consumed by various components in structural systems. These components can be assumed as responses to the effect of the input energy on the building. Regarding the associated components, it is defined as the kinetic energy (E_K) related to the mass, the damping energy (E_D) related to the damping ratio, and the total energy (E_A) consumed in elastic and plastic behavior (Eq. 20).

$$E_K + E_D + E_A = E_I \qquad (20)$$

The elastic strain energy (E_S) and plastic strain energy (E_H) (non-recoverable hysteretic energy), which are the two components of the total energy (E_A) can be written separately in Eq. (21). If the hysteretic energy (E_H) becomes zero, then it means that the structure exhibits linear elastic behavior (Benavent-Climent et al. 2010).

$$E_K + E_D + [E_S + E_H] = E_I \qquad (21)$$

5.2 Sample results

Samples of energy curves for SDOF and MDOF systems of 4- and 7-story buildings are given in Fig. 7 in order to see energy changes for the Chuetsu-65035ew record at the design earthquake (DD-2) level. It can be seen that the elastic (E_S) and kinetic (E_K) energies constitute much less of the input energy (E_I) than the hysteresis (E_H) and damping (E_D) energies. The energy in the structure is consumed mostly as hysteresis energy, followed by damping energy. The hysteresis and damping energy show a similar trend to the input energy, whereas other energies are separated from them. Based on the figures presented below, the energy values obtained in the 4-story model with SDOF are higher when compared to the MDOF system, whereas the values of the 7-story model with SDOF are lower in comparison to the MDOF system. In terms of the story numbers, the amount of energy calculated for the 7-story model is higher than that of the 4-story model.

6 Discussion of results

The energy and displacement values were obtained from nonlinear time history analyses of 4- and 7- story buildings for SDOF and MDOF systems. Input energy, hysteretic energy, distribution of hysteretic energy to floors and structural elements calculated
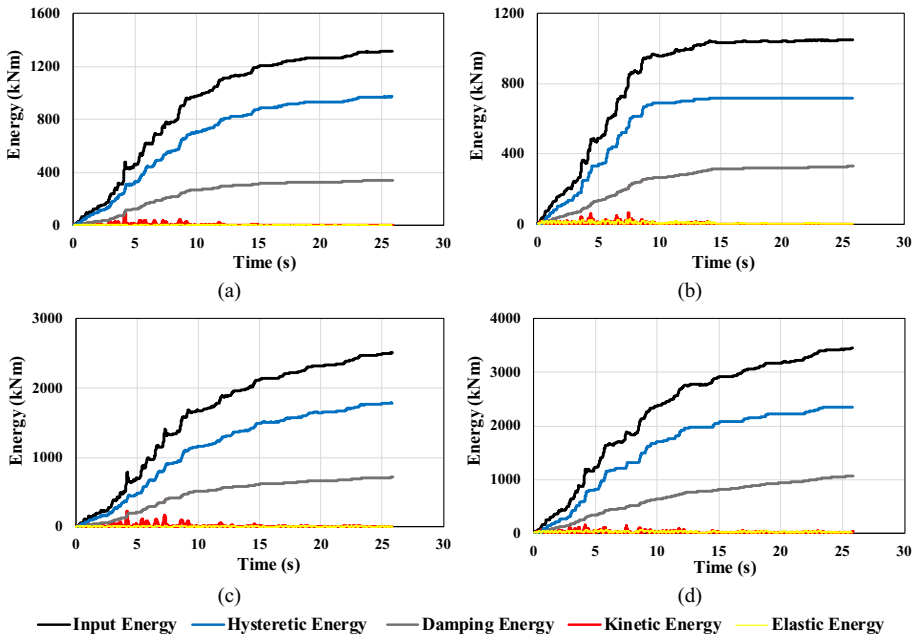
Fig. 7 The variation of energy parameters with time for Chuetsu-65035ew record: **a** for the 4-story model with SDOF, **b** MDOF, **c** for 7-story model with SDOF and **d** MDOF

from analyses with design (DD-2) and maximum (DD-1) ground motions were examined. The relationship between input energy and hysteretic energy was examined separately according to the selected ground motion records. In addition, the intercourse between roof drift and input energy was studied in terms of SDOF and MDOF systems.

The correlation coefficient is used as a linear function to reveal the relationship between the parameters within the scope of the study (Palanci and Senel 2019). The degree of dependence between the variables depending on the correlation coefficients is presented in detail in Table 5. Determination coefficient is used to interpret how much of the observed variability in one variable is explained by the other variable and it is equal to the square of the correlation coefficient. The correlation coefficient is denoted by R, while the determination coefficient is expressed as R^2. The correlation coefficient between two variables X and Y is given by Eq. (22):

Table 5 Degrees of relationship corresponding to the correlation range

Correlation range	Relation level
-0.25 to -0.00 and 0.00 to 0.25	Very weak
-0.49 to -0.26 and 0.26 to 0.49	Weak
-0.69 to -0.50 and 0.50 to 0.69	Middle
-0.89 to -0.70 and 0.70 to 0.89	High
-1.00 to -0.90 and 0.90 to 1.00	Very high

$$R(X, Y) = \frac{\sum\limits_{i=1}^{N} (X_i - \overline{X})(Y_i - \overline{Y})}{\sqrt{\sum\limits_{i=1}^{N} (X_i - \overline{X})^2 \sum\limits_{i=1}^{N} (Y_i - \overline{Y})^2}} \tag{22}$$

where $\overline{X}$ and $\overline{Y}$ are the average values of X_i and Y_i respectively, and N is the number of couple of values (X_i, Y_i) in the equation.

6.1 Input and hysteretic energy

Ground motion records used in the nonlinear analyses revealed inelastic behaviors in SDOF and MDOF models and hysteretic energy, which is an indicator of damage, was released. Hysteretic energy is consumed by the formation of plastic hinges in structural members for MDOF buildings. Hysteretic energy is generated in SDOF systems using period, strength ratio, and post-yield stiffness ratio by nonlinear time history analysis of SDOF models. The acceleration values of the maximum ground motions that are higher than the design earthquakes increase the intensity of the records and the structural input energy.

The input energy is significantly affected by the characteristics of the ground motions. Table 6 shows that the lowest and highest energies were found in the Chichi-chy101n and Chuetsu-65035ew records for two earthquake levels in the 4-story model, respectively. In the 7-story building, the highest values were found in the Chuetsu-65035ew in both SDOF and MDOF, whereas the lowest results were found in Chichi-chy101n for SDOF and Iwate-54015 ns for MDOF as can be seen in Table 7. The acceleration values and effective duration of the Chuetsu-65035ew are higher than the other two records provided an important increment in both hysteretic energy (E_H) and input energy (E_I). However, no parallel trend was observed between the increase and decrease of energy amount and the E_H/E_I ratios.

The hysteretic energy (E_H) and input energy (E_I) values of the maximum earthquakes were divided by the design ground motion values in order to understand the effects of earthquake levels on the analysis results. In addition, the SDOF values were normalized with MDOF ones to determine the changes of one- and three-dimensional modeling on the results. The E_H and E_I mean values of the maximum records for the SDOF system are approximately 2.8 folds of the design data. The DD-2/DD-1 ratio was calculated to be 3.35 and 2.83 for E_H and E_I, respectively, in the 4-story model for the MDOF system, whereas it was found to be 2.86 and 2.49 for the 7-story building. Although the difference between the energy ratios in terms of the earthquake levels is the same for the 4- and 7-story models in the SDOF system, lower values were obtained in the 7-story building model for the MDOF.

For the 4-story model of the SDOF system, the E_H and E_I values of the design earthquakes are 37% and 10% more than the MDOF, while they are 15% and 9% higher per the results based on the maximum records. When the comparison is made for 7-story building in the same way, 9% increase for E_H and 8% decrease for E_I is calculated for design records. According to the data of maximum earthquakes, 7% and 4% increments are obtained for E_H and E_I, respectively. Given the results achieved here, it can be said that there is an increasing trend for both 4- and 7- story models, except for the E_I value of the 7-story model for the SDOF/MDOF ratio. Evaluating the difference between the models in terms of story number, the E_H and E_I values for the design earthquakes of the 7-story model for the MDOF system are 2.40 and 2.32 times, respectively, the 4-story building, whereas it is approximately 2 times for maximum earthquakes. It

Table 6 Energy values of the 4-story building model

Earthquakes	SDOF						MDOF					
	DD-2			DD-1			DD-2			DD-1		
	E_H (kNm)	E_I (kNm)	E_H/E_I	E_H (kNm)	E_I (kNm)	E_H/E_I	E_H (kNm)	E_I (kNm)	E_H/E_I	E_H (kNm)	E_I (kNm)	E_H/E_I
Chalfant-lad180	290.84	387.17	0.75	814.10	1083.74	0.75	233.98	365.23	0.64	710.67	989.61	0.72
Chalfant-lad270	217.89	311.78	0.70	609.91	872.73	0.70	205.95	360.44	0.57	584.59	902.91	0.65
Chichi-chy101e	241.82	321.54	0.75	676.84	899.97	0.75	121.26	253.68	0.48	421.97	678.11	0.62
Chichi-chy101n	156.61	212.77	0.74	438.34	595.54	0.74	93.63	180.33	0.52	382.71	579.44	0.66
Chuetsu-65035ew	971.07	1315.88	0.74	2718.18	3683.37	0.74	717.71	1049.87	0.68	2613.07	3463.31	0.75
Chuetsu-65035 ns	750.78	1052.35	0.71	2101.56	2945.71	0.71	701.78	1022.46	0.69	2067.48	2822.30	0.73
Darfield-dfhss17e	387.96	519.39	0.75	1085.89	1453.76	0.75	201.27	440.39	0.46	815.81	1256.15	0.65
Darfield-dfhss73w	480.99	670.02	0.72	1346.29	1875.38	0.72	463.16	814.90	0.57	1290.16	1919.79	0.67
El mayor-r000	333.29	465.36	0.72	932.93	1302.61	0.72	254.51	521.06	0.49	860.89	1368.89	0.63
El mayor-r090	414.89	589.22	0.70	1161.33	1649.29	0.70	327.32	640.52	0.51	1208.60	1847.51	0.65
Impvall-chi012	667.84	916.74	0.73	1869.37	2566.08	0.73	572.00	869.61	0.66	1706.39	2394.28	0.71
Impvall-chi282	767.74	1088.49	0.71	2149.01	3046.82	0.71	666.82	928.75	0.72	2120.54	2851.87	0.74
Impvall-elc180	575.61	789.12	0.73	1611.20	2208.83	0.73	362.98	673.74	0.54	1260.97	1855.77	0.68
Impvall-elc270	412.06	578.05	0.71	1153.40	1618.03	0.71	273.44	537.65	0.51	1002.17	1539.82	0.65
Iwate-54015ew	418.08	551.61	0.76	1170.22	1543.99	0.76	302.11	474.99	0.64	938.05	1296.76	0.72
Iwate-54015 ns	262.44	342.00	0.77	734.58	957.27	0.77	73.76	190.51	0.39	364.93	582.02	0.63
Kobe-abnt000	339.17	480.59	0.71	949.41	1345.29	0.71	204.59	442.59	0.46	730.24	1184.28	0.62
Kobe-abnt090	266.21	397.00	0.67	745.20	1111.31	0.67	146.08	398.68	0.37	519.10	977.72	0.53
Northridge-ro3000	361.28	495.41	0.73	1011.18	1386.61	0.73	348.81	598.37	0.58	1101.52	1578.99	0.70
Northridge-ro3090	485.90	689.19	0.71	1359.97	1928.96	0.71	375.14	563.49	0.67	1159.03	1641.95	0.71
Supersition-wsm090	223.84	302.20	0.74	626.51	845.82	0.74	94.11	268.60	0.35	418.85	724.61	0.58
Supersition-wsm180	491.03	711.49	0.69	1374.33	1991.40	0.69	191.72	367.66	0.52	978.97	1382.27	0.71
Mean	432.61	599.43	0.72	1210.90	1677.84	0.72	315.10	543.80	0.55	1057.12	1538.11	0.67

Table 7 Energy values of the 7-story building model

| Earthquakes | SDOF | | | | | | MDOF | | | | | |
| | DD-2 | | | DD-1 | | | DD-2 | | | DD-1 | | |
	E_H (kNm)	E_I (kNm)	E_H/E_I	E_H (kNm)	E_I (kNm)	E_H/E_I	E_H (kNm)	E_I (kNm)	E_H/E_I	E_H (kNm)	E_I (kNm)	E_H/E_I
Chalfant-lad180	635.09	855.77	0.74	1777.71	2395.42	0.74	585.43	909.50	0.64	1620.60	2271.03	0.71
Chalfant-lad270	379.15	553.64	0.68	1061.29	1549.73	0.68	204.76	420.35	0.49	1044.89	1548.24	0.67
Chichi-chy101e	612.00	843.67	0.73	1712.95	2361.38	0.73	191.77	436.11	0.44	760.65	1192.60	0.64
Chichi-chy101n	340.18	450.48	0.76	952.13	1260.87	0.76	273.78	521.61	0.52	774.96	1241.32	0.62
Chuetsu-65035ew	1782.76	2503.52	0.71	4990.22	7007.76	0.71	2348.90	3447.07	0.68	5544.52	7682.68	0.72
Chuetsu-65035 ns	1400.81	1980.93	0.71	3921.10	5544.97	0.71	1952.75	2998.73	0.65	4591.44	6480.30	0.71
Darfield-dfhss17e	869.57	1184.02	0.73	2433.92	3314.04	0.73	547.19	1072.37	0.51	1986.09	2929.46	0.68
Darfield-dfhss73w	695.02	1009.60	0.69	1945.36	2825.86	0.69	550.42	1113.57	0.49	1815.95	2835.58	0.64
El mayor-r000	610.81	857.67	0.71	1709.73	2400.71	0.71	430.37	889.41	0.48	1505.46	2385.25	0.63
El mayor-r090	616.58	901.09	0.68	1725.89	2522.27	0.68	735.82	1331.79	0.55	2057.75	3190.70	0.64
Impvall-chi012	1232.77	1706.42	0.72	3450.66	4776.49	0.72	1446.73	2197.84	0.66	3462.21	4907.45	0.71
Impvall-chi282	1351.89	1936.30	0.70	3784.09	5419.95	0.70	1817.72	2604.76	0.70	4333.62	5935.95	0.73
Impvall-elc180	1003.10	1444.15	0.69	2807.78	4042.33	0.69	980.04	1636.27	0.60	2782.93	3980.07	0.70
Impvall-elc270	754.42	1071.51	0.70	2111.70	2999.28	0.70	490.19	963.94	0.51	1657.69	2537.84	0.65
Iwate-54015ew	932.92	1258.57	0.74	2611.28	3522.77	0.74	586.18	953.96	0.61	1844.76	2581.11	0.71
Iwate-54015 ns	779.67	1088.76	0.72	2182.34	3047.49	0.72	157.67	357.88	0.44	753.23	1117.39	0.67
Kobe-abn000	642.09	922.70	0.70	1797.37	2582.85	0.70	428.24	823.17	0.52	1638.90	2523.88	0.65
Kobe-abn090	626.47	928.87	0.67	1753.64	2600.14	0.67	153.77	488.11	0.32	1003.57	1785.76	0.56
Northridge-ro3000	585.64	820.18	0.71	1639.13	2295.58	0.71	689.71	1186.97	0.58	1882.52	2737.42	0.69
Northridge-ro3090	993.52	1408.97	0.71	2780.76	3943.56	0.71	926.32	1379.16	0.67	2513.43	3537.30	0.71
Superstition-wsm090	486.45	664.19	0.73	1361.52	1859.00	0.73	287.65	647.94	0.44	1184.91	1836.09	0.65
Superstition-wsm180	873.27	1291.81	0.68	2444.19	3615.63	0.68	843.53	1396.10	0.60	2831.61	3925.08	0.72
Mean	827.46	1167.40	0.71	2316.13	3267.64	0.71	755.86	1262.57	0.55	2163.26	3143.75	0.67

should be noted that it ensures the energy to be high due to the mass of the 7-story building is approximately 2 times higher than the 4-story building, which affects the input energy more than other structural features (period, stiffness, and ductility, etc.).

Many researchers made an effort to obtain stable trends for the ratio of hysteretic energy to input energy (E_H/E_I) (Benavent-Climent et al. 2010; Dindar et al. 2015; Fajfar and Vidic 1994; Khashaee et al. 2003; Okur and Erberik 2014). The E_H/E_I ratio for SDOF systems was calculated to be 0.72 and 0.71 using the average values, respectively, in 4- and 7-story buildings, which shows that similar conclusions were obtained with the $E_H/E_I = 0.7$ value suggested by Fajfar and Vidic (1994) and Okur and Erberik (2014). Given the analysis results with design earthquakes considering MDOF systems, the E_H/E_I ratio is 0.55 for both 4- and 7-story buildings, which is lower than the SDOF results. The value of 0.67 calculated using the maximum ground motions reveals that the E_H/E_I data of the MDOF approach the SDOF as the earthquake level increases. Although the E_H/E_I ratio has different values for SDOF and MDOF systems, it was observed that it had almost the same average values for 4- and 7-story models.

The input energy is affected by both the structural features and the characteristics of the ground motions. Therefore, as the ground motion and structural system change, it is clear that there will be differences in parameters such as input energy and hysteretic energy. Structural damage occurs in direct proportion to hysteretic energy. In the building where damage started to occur, it consumes hysteretic energy by exhibiting inelastic behavior at the end regions of the structural elements. Hence, it can be expected that the damage occurrence will vary between 4- and 7-story buildings depending on the structural features with the selected earthquakes. As can be seen in Fig. 8, majority of the hysteretic energy is consumed in the first three and five floors for 4- and 7-story buildings, respectively. The floors, except for the aforementioned floors, generally exhibited elastic behavior. The increase in the earthquake level for both building groups does not create any significant difference in the distribution of hysteretic energy.

As a requirement of the capacity design approach, with the principle of "strong column-weak beam", a significant part of the earthquake energy is expected to be consumed by the plastic hinges of the beams. The formation of plastic hinges primarily at the beam ends ensures that the structure system behaves ductile. Redistribution occurs and load transfer happens between neighboring elements because of the ductile behavior. Thus, sudden collapse mechanisms are prevented and plastic hinges are formed in more structural elements. At the same time, more earthquake energy is absorbed when ductile damage occurs. As can be seen from Fig. 9, the fact that majority of the hysteretic energy emerges in the beams relative to the columns is an indication of compliance with the relevant capacity design principle. For design earthquakes, approximately 90 and 95% of the hysteretic energy was generated in the beams of 4- and 7-story buildings, respectively. By using the maximum earthquakes, the hysteretic energy consumed in the columns was increased by 10% and 5% for the 4- and 7-story models. Since the spectral acceleration values corresponding to the period of the 4-story building are generally higher on the spectrum of earthquakes selected in accordance with the response spectra, the 4-story building was exposed to more earthquake loads on a floor basis. Therefore, since the columns of the 4-story building were more damaged than the 7-story model, the share of hysteretic energy in consumption increased.
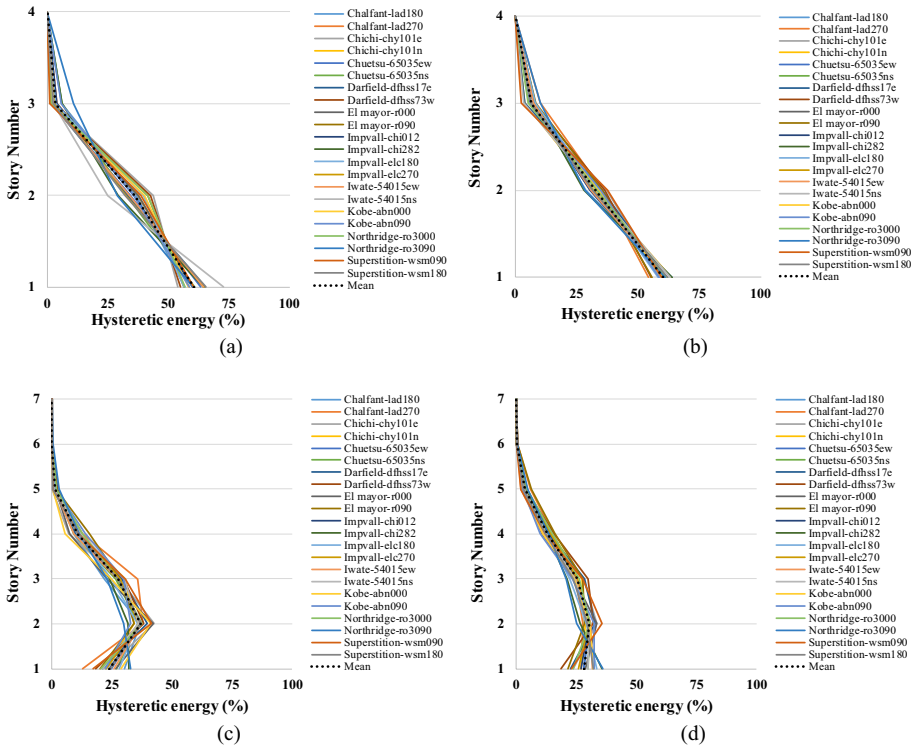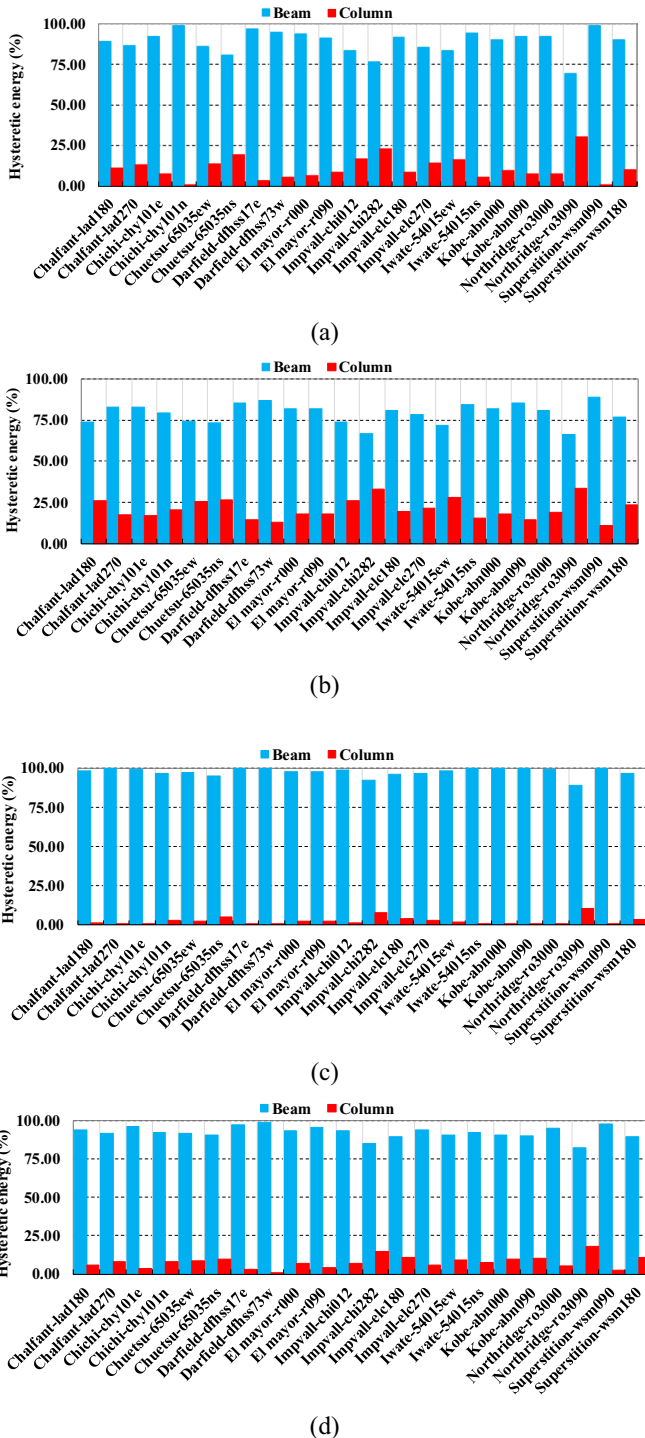
Fig. 8 Distribution of hysteretic energy to floors: **a** in the 4-story model for DD-2, **b** DD-1 earthquake levels, **c** in the 7-story model for DD-2 and **d** DD-1 earthquake levels

6.2 Relationship between roof drift and input energy

Many researchers carried out studies in order to determine the relationship between displacement and energy demands (Fabrizio et al. 2011; Hori and Inoue 2002; Ye and Otani 1999). For this purpose, the parameters for specific ductility and period intervals were calculated by using the energy and displacement values obtained from the analyses of SDOF systems. Based on these parameters, various spectra were proposed by those researchers. In the present study, variables such as energy and displacement were compared over four correlations: roof drifts (SDOF-MDOF), energy values (SDOF-MDOF) and roof drifts-energy values (separately for SDOF and MDOF). In order to evaluate the buildings as a whole, the percentage of these values is taken after the roof displacements are divided by building height and entitled as "roof drift ratio (%)", input energies are normalized by masses of buildings and entitled as "$(E_I/m)[m^2/s^2]$" (Fig. 10). Once input energies are normalized by mass, they can also be expressed in equivalent velocities (Benavent-Climent et al. 2010).

The correlation between the input energy values obtained from the SDOF and MDOF is higher in comparison to the roof drifts. The relationship between roof drifts and input energy data is underestimated for both SDOF and MDOF systems. The medium correlation (approximately R≈0.65) between energy and drift values can be attributed to the cumulative calculation of the energy data, although the displacement values are obtained instantaneously.

(a)

(b)

(c)

(d)

Fig. 9 Distribution of hysteretic energy to structural elements: **a** in the 4-story model for DD-2, **b** DD-1 records, **c** in the 7-story model for DD-2 and **d** DD-1 records
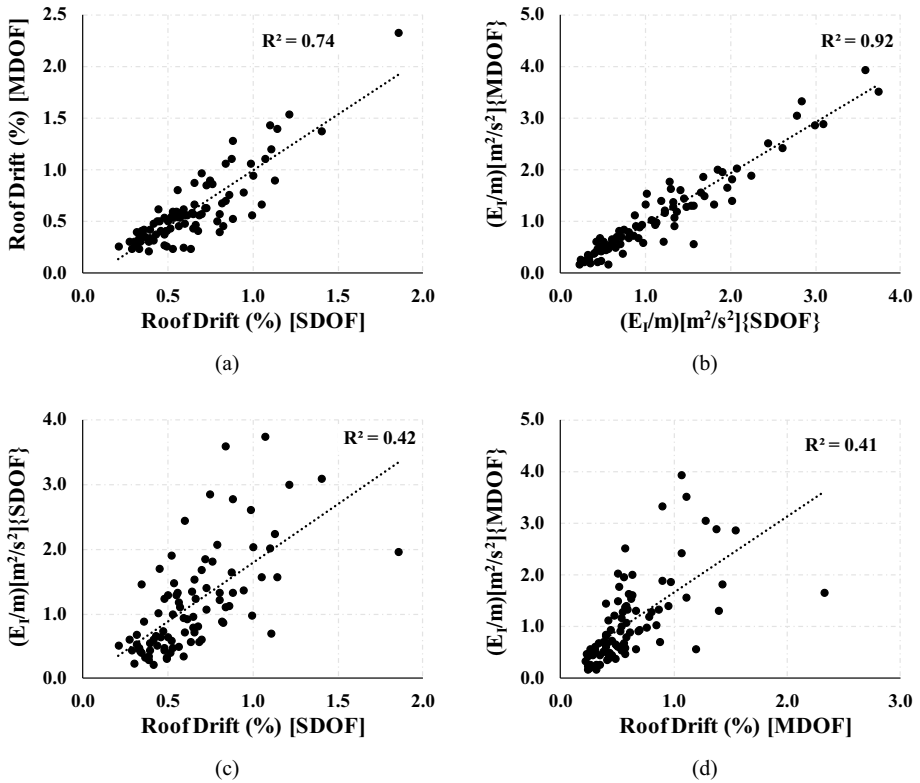
Fig. 10 The comparison of displacement and energy demands: **a** roof drifts, **b** input energies, **c** roof drifts–input energies for SDOF and **d** MDOF

7 Correlation between GMPs with input energy

7.1 Single parameter correlation

Evaluation of the damage status of the structures is carried out in two ways, before and after the earthquake. In the first case, the damage to the structure is determined analytically by using seismic analysis methods, considering the dynamic properties of the structure and earthquake scenarios. In the second case, damage assessment of the building is performed by using the rapid seismic assessment methods that take into account the observational determination of structural defects, which affect the seismic performance of the building by street scans. Although the first stage includes the damage estimation of the undamaged structure, the second stage covers the investigations after the damage has occurred. So, if the structure is seismically inadequate, then it might be too late for the second stage. Whichever parameter of the earthquake considered in this study is more related to the input energy will provide a preliminary idea about the estimation of the damage without calculation. At the same time, it is thought that the level of damage will indicate the performance of the building against the earthquake and shed light on situations such as whether the building can be repaired and strengthened, if necessary, deciding to demolish the building.

The aim of the correlation of energy values and ground motion parameters (GMPs) in the present study is to determine the parameters that best reflect the potential damage that may occur under future earthquake hazards. For this purpose, the relationship between the considered parameters and the input energy is calculated with the correlation coefficients (R) and transferred to table numerically. In addition, linear trend line and determination coefficient (R^2) are added to the sample graphs in order to have information about the variation of energy with the magnitudes of the parameters.

The separation of buildings as 4- and 7-story is to see the effects of mass and period on the energy-earthquake parameter relationship rather than the number of floors. Even though the mass directly affects the energy demands, the period is also affected as it is dependent on the mass. Moreover, even if the buildings have different numbers of floors, they might have the same mass and period due to the structural characteristics of the buildings. Within the scope of this study, the variation of these on the correlation is examined by providing diversity in terms of mass and period.

In order to combine the energy demands with different floor numbers, the energy values independent from the mass are determined by normalizing the input energy demands with the building mass. The relationship between these energy data and GMPs is transformed such that all buildings can be evaluated only in terms of SDOF and MDOF systems. Then, the dual correlation values of SDOF and MDOF are converted into a single value in order to understand the difference between the parameters more clearly.

Correlation of the parameters with the energy demands of building models with different numbers of floors, SDOF-MDOF systems, and a combination of all are given in Table 8. Besides, parameters are given in 4 groups under the "Type" column as acceleration, velocity, frequency, and displacement. The parameters in each group are listed from largest to smallest depending on the correlation coefficient in the last column where all are combined. It was preferred to group the parameters in order to clearly see whether the parameters related to the same type are dominant when compared to other types.

The correlation coefficients of the parameters in the acceleration group for the 7-story building were found to be 5% lower than the 4-story model. The biggest differences in terms of the number of floors were obtained for T_m and V_{max}/A_{max}, whereas the results of other parameters were close to each other. From a modeling perspective, the correlation values of SDOF are approximately 20% higher than MDOF. Parameters related to acceleration and velocity (except V_{rms} and SED) were found to have a higher correlation when compared to the ones that are related to frequency and displacement.

I_a, I_c, A_{rms}, and SMA as acceleration-related parameters have the best values, whereas VSI, HI, and CAV have a good correlation in the velocity group. They have correlation coefficients ranging between 0.7 and 0.9. Even though ASI, EDA, PGA, and A95 exhibited moderate correlations in the acceleration group, similar results were found in the SMV and PGV parameters of the velocity group. Given these results, it can be stated that more acceleration-parameters give good results compared to other groups.

In accordance with the nature of the energy amount calculation, the parameters obtained cumulatively by integral showed a generally good correlation, whereas the instantly-calculated parameters demonstrated a moderate correlation. For the V_{rms} parameter, very low and good correlations were obtained by Riddell and Garcia (2001), Riddell (2007) for the 0.2 and 1 s periods of the SDOF system, respectively. Since the periods (0.50 and 0.67 s) of the buildings in the present study are between the periods used by them, the low correlation values obtained are acceptable for the V_{rms}. Although the energy expression is mentioned in the SED parameter, the weak correlation with the input energy stands out as a very surprising result, contrary to expectation.

Table 8 Correlation coefficients (R) of parameters with input energy values of building models according to different cases

Type	Parameter	4-story		7-story		All Systems		All Buildings		All
		SDOF	MDOF	SDOF	MDOF	4-story	7-story	SDOF	MDOF	
Acceleration	I_a	0.885	0.901	0.856	0.818	0.891	0.835	0.871	0.856	0.863
	I_c	0.876	0.886	0.857	0.804	0.879	0.828	0.866	0.842	0.853
	A_{rms}	0.783	0.786	0.784	0.708	0.783	0.743	0.783	0.744	0.763
	SMA	0.735	0.737	0.741	0.646	0.734	0.690	0.737	0.688	0.712
	ASI	0.677	0.707	0.642	0.605	0.690	0.621	0.659	0.652	0.655
	EDA	0.669	0.666	0.693	0.590	0.666	0.637	0.680	0.625	0.652
	PGA	0.667	0.667	0.689	0.585	0.666	0.633	0.677	0.623	0.649
	A95	0.664	0.663	0.686	0.582	0.662	0.630	0.674	0.619	0.646
Velocity	VSI	0.886	0.825	0.920	0.845	0.854	0.879	0.902	0.834	0.867
	HI	0.846	0.770	0.900	0.787	0.807	0.839	0.871	0.777	0.823
	CAV	0.741	0.754	0.708	0.684	0.745	0.694	0.725	0.716	0.720
	SMV	0.606	0.552	0.662	0.509	0.578	0.581	0.632	0.528	0.579
	PGV	0.550	0.495	0.637	0.447	0.522	0.536	0.591	0.469	0.529
	V_{rms}	0.331	0.280	0.412	0.218	0.305	0.309	0.370	0.247	0.307
	SED	0.285	0.256	0.331	0.183	0.271	0.253	0.307	0.218	0.262
Frequency	T_p	0.371	0.374	0.303	0.477	0.372	0.394	0.338	0.427	0.383
	T_m	0.153	0.029	0.258	0.161	0.093	0.206	0.204	0.098	0.150
	V_{max}/A_{max}	−0.118	−0.178	−0.060	−0.158	−0.147	−0.112	−0.090	−0.167	−0.129
Disp.	PGD	0.158	0.124	0.219	0.076	0.141	0.144	0.187	0.099	0.142
	D_{rms}	0.151	0.119	0.215	0.071	0.135	0.139	0.182	0.093	0.137

None of the displacement and frequency-related parameters have notable results. Although T_p is one step ahead in the frequency group, it shows a poor correlation. Unlike other parameters, V_{max}/A_{max} has a very low relationship in the reverse direction (negative correlation). It is not possible to use parameters such as T_m, V_{max}/A_{max}, PGD, and D_{rms} alone as damage indicators.

Since it is difficult to make observations and comments on the figures about parameters with low correlation, the relationships of parameters that correlate better with input energy are shown in Figs. 11 and 12 through sample graphs. The increment in intensity of ground motion increases both the amount of the energy used as damage measure (DM) and the value of earthquake parameters considered as intensity measure (IM). The increase in the energy and parameters caused by the earthquake does not change at the same rate as the intensity of ground motion. Therefore, it can be concluded that the point data in the related graphs move away from the trend line and the correlation of the parameters considered decreases as the intensity of seismic excitations increases.

The distribution of I_a and VSI parameters, which have the strongest correlation with energy, varies in a narrower range when compared to other parameters. It is clearly seen in Figs. 11 and 12, as well as in Table 8, that the values of SDOF are compatible with MDOF ones and the data do not deviate much from each other.

The R^2 values of the parameters are ranked in Fig. 13 by evaluating all buildings together in terms of SDOF and MDOF. Even though the place of the parameters changes in arrangement, the parameter with a low determination coefficient of SDOF does not have a high value for MDOF. Therefore, it can be concluded that SDOF and MDOF follow a parallel trend.

7.2 Multi parameter correlation

In order to increase the correlation obtained from the parameters within the scope of the present study and to reduce the scattering, the use of multiple parameters together instead of just one parameter was also examined. For this reason, different equations for SDOF and MDOF were discussed in order to combine parameters. In order to find the equations, it is aimed to obtain the highest correlation by using the least number of parameters. As a result of linear regression analyses performed for this purpose, Eqs. (23) and (24) were derived separately for SDOF and MDOF, respectively.

In multiple regression analyses, relevant equations with 6 and 5 parameters were created for SDOF and MDOF, respectively, according to conditions such as P-value (Significance Value) < 0.05 and VIF (Variance Inflation Factor) < 10. When all of 20 GMPs are taken into account, the correlation coefficients are calculated as 0.981 and 0.975 for SDOF and MDOF, respectively, and these values are obtained as 0.945 and 0.937 via the equations (Fig. 14). Although there is a decrease of approximately 4% in the correlation coefficients obtained with the equations compared to all parameters, the energy amount can be easily calculated with fewer parameters by reducing the number of variables.

VSI and I_a parameters reflect the damage potential of earthquakes as the best single parameter for SDOF and MDOF, respectively. The correlation coefficients of these parameters were previously calculated to be 0.902 and 0.856, and these values were improved with an increase by 5 and 10% thanks to multiple regression. It is noteworthy that, although parameters such as PGV and D_{rms} do not have a high correlation on their own, they are included in the equations together with the VSI and I_a parameters.
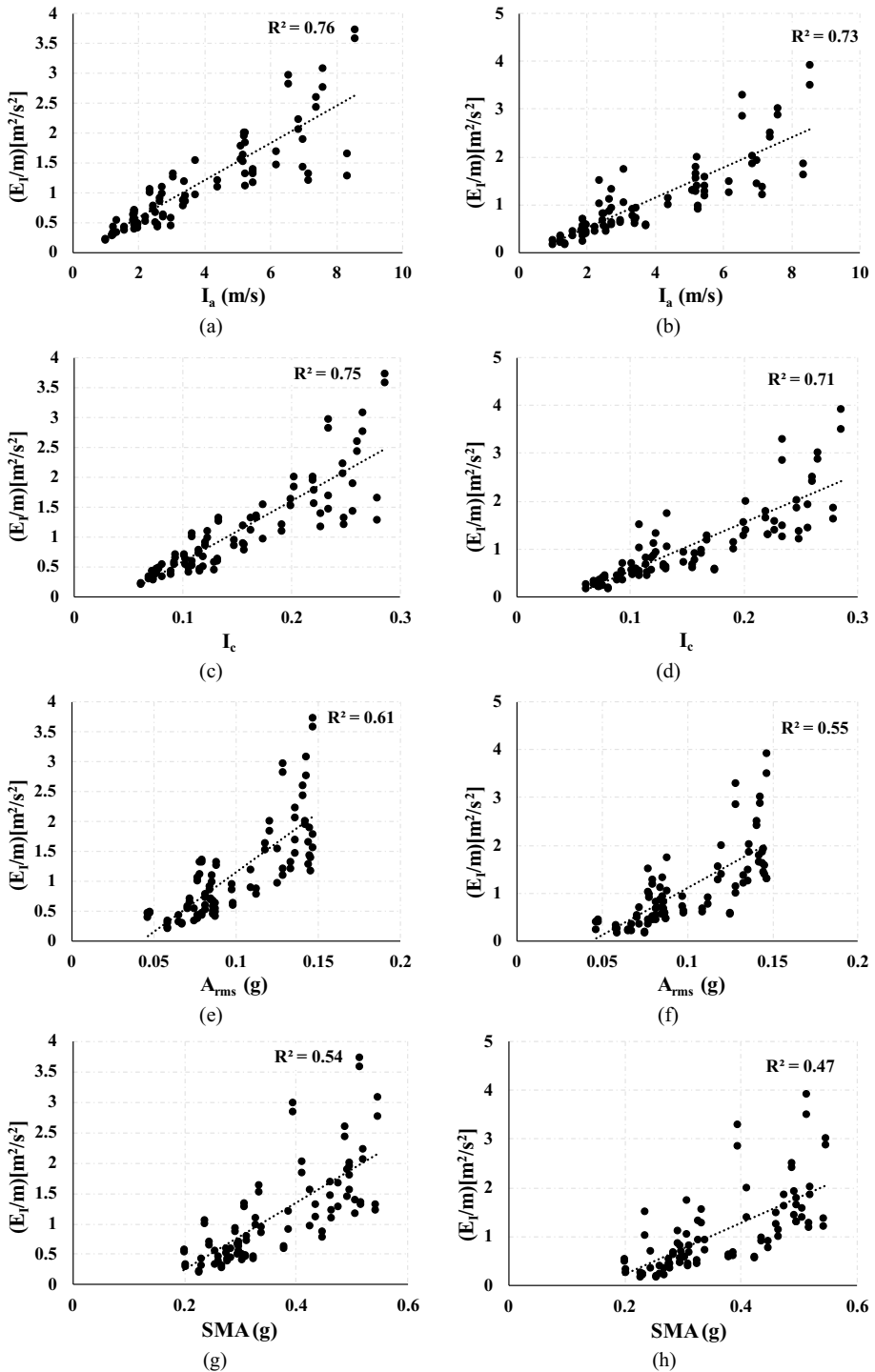
Fig. 11 Relation of some acceleration-related parameters with energy values for all buildings: left side for SDOF and right side for MDOF
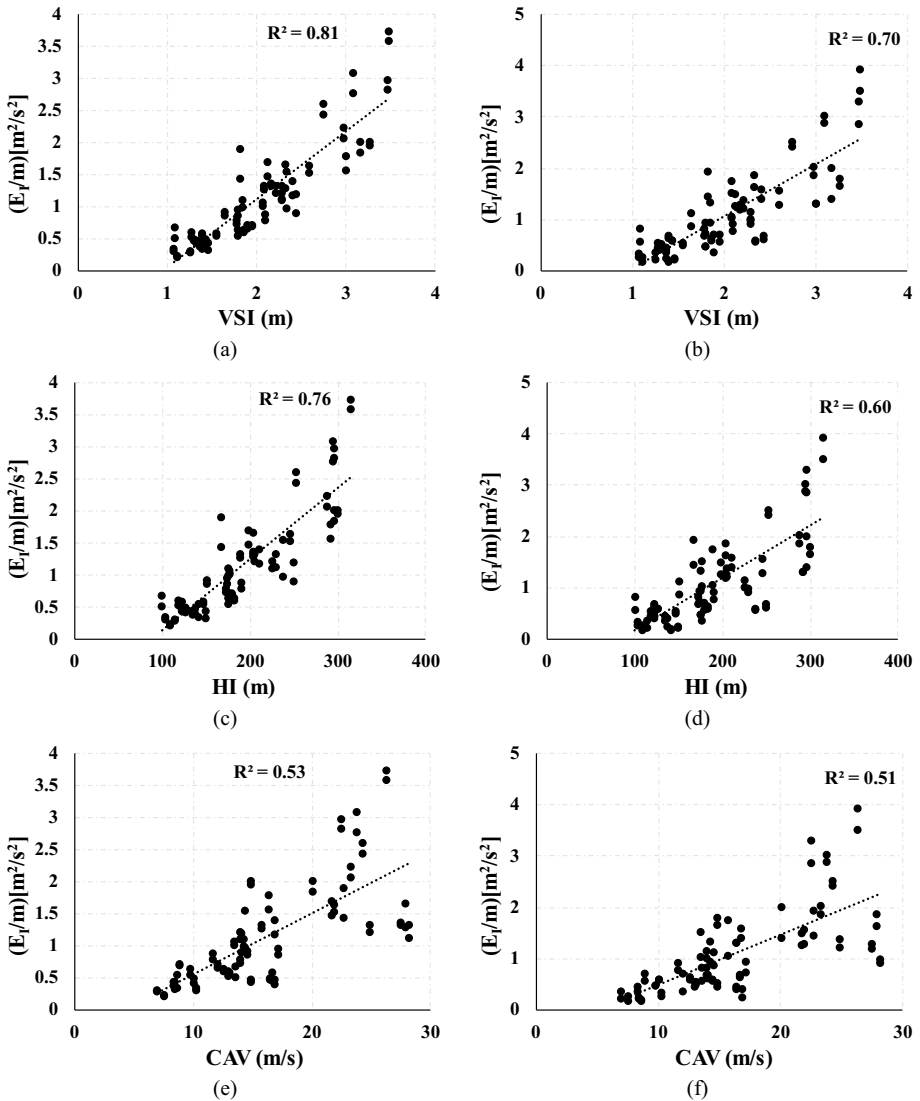
Fig. 12 Relation of some velocity-related parameters with energy values for all buildings: left side for SDOF and right side for MDOF

$$E_I(m^2/s^2) = -1.088 - 1.012PGV + 7.61A_{rms} + 0.04283CAV - 1.793ASI + 0.8761VSI + 0.763A95$$

$$(23)$$

$$E_I(m^2/s^2) = -0.629 - 1.636PGV + 0.1208D_{rms} + 0.2439I_a + 0.00628HI + 1.319T_p$$

$$(24)$$

While the input energy estimation can be made through the equations generated, the amount of hysteretic energy can be calculated approximately by using the E_H/E_I ratios, which were previously found separately for SDOF and MDOF systems. While getting
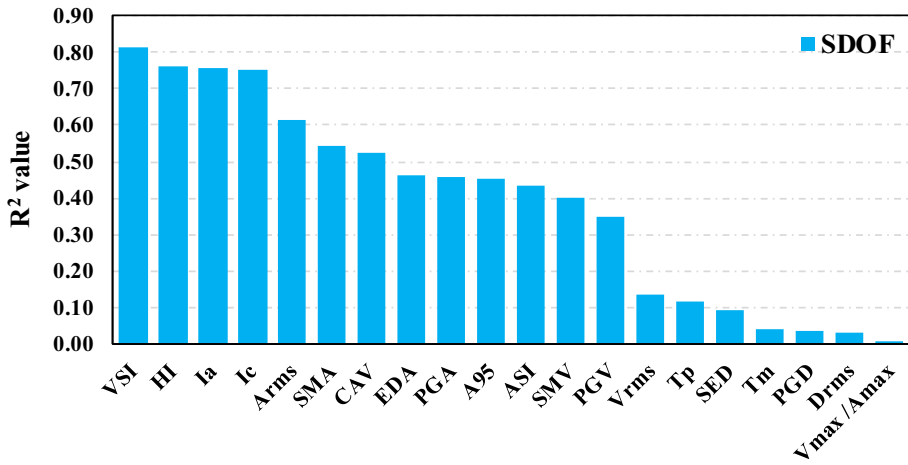
(a)
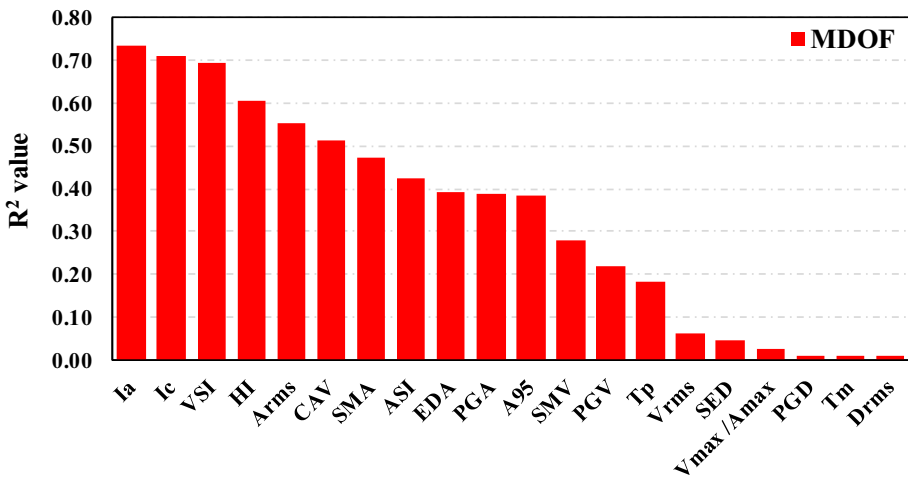
(b)

Fig. 13 R^2 values for GMPs of all models: **a** for SDOF and **b** MDOF systems

an idea about the amount of input energy with the equations used in the current study, it also shows that there is a significant relationship between the relevant parameters and energy demands.

Since it aims to provide preliminary information about the correlation of the combined parameters and the energy amount with the created equations, many different equations can be derived with various assumptions and additional parameters. It should be kept in mind that the literature can be enriched by expanding the scope due to the
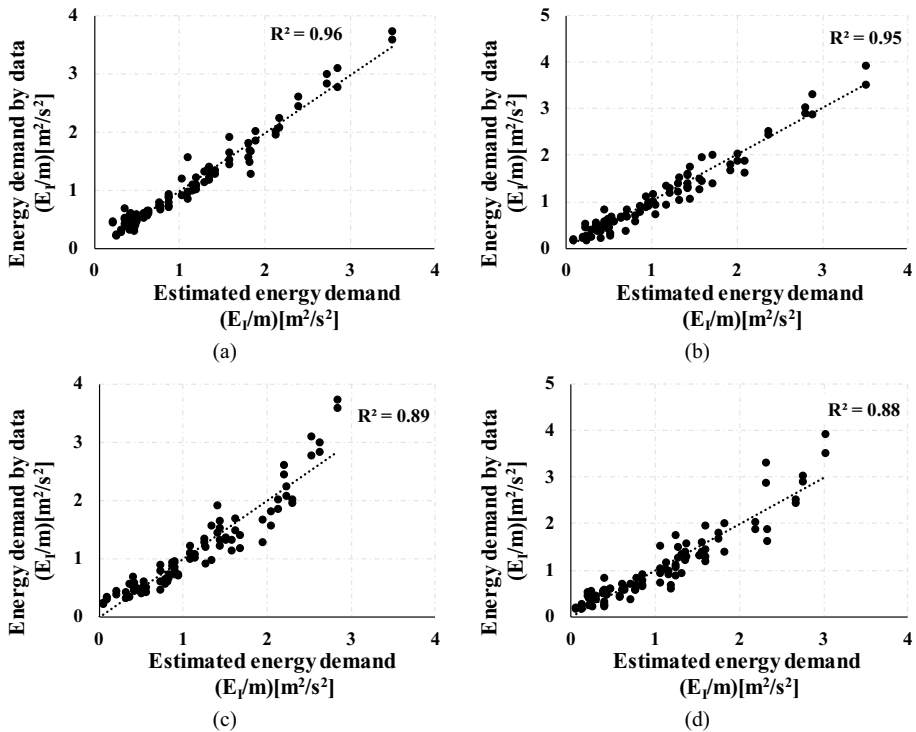
Fig. 14 The relationship between energy demands estimated by ground motion parameters and obtained from the analysis results: **a** for 20 GMPs with SDOF, **b** MDOF, **c** for selected parameters with SDOF and **d** MDOF

proposed equations are limited to the models, the number of earthquakes and the parameter type in the study.

8 Conclusions

Seismic loads play a crucial role among the loads considered in the design of earthquake-resistant structures and evaluation of existing buildings. There are many studies highlighting the different properties of ground motion records in order to predict the structures' response under seismic loads. This study investigates the correlation of ground motion parameters (GMPs) with energy demands of low-rise reinforced concrete buildings without shear walls. For this purpose, 4- and 7-story buildings without any irregularity were modeled in order to represent low-rise structures. In order to obtain the demands of SDOF systems as well as MDOF systems, the properties of "equivalent" SDOF systems were determined by using MDOF systems. For design and maximum earthquake levels, 44 ground motion records in total, 22 pairs in compliance with the Turkish Building Earthquake Code (TBEC 2018), were selected and scaled. Twenty GMPs were used for each of the records depending on different variables (e.g., acceleration, velocity, displacement, and frequency). Input energy data are considered as demand measure and these values are normalized with the masses of the buildings for

cases where the buildings are evaluated together. The correlation between input energy results and GMPs is also investigated in terms of the number of floors and modeling. The correlation of 20 GMPs of 44 records with the energy demands obtained from a total of 176 nonlinear time history analyses was examined for the present study. The significant achievements and outcomes gained within the scope of this study are summarized below:

- Evaluating all earthquakes, it was determined that the input energy values of the 4-story model with SDOF were 10% higher than the MDOF, whereas the values of SDOF and MDOF for the 7-story model were close to each other. In terms of the correlation coefficient, the SDOF values for all parameters were found to be approximately 20% higher than MDOF. Considering the amount of energy and correlation values, it can be said that MDOF is successfully represented by SDOF.
- While the biggest differences in terms of the number of floors were found in the frequency-related T_m and V_{max}/A_{max} parameters, the correlation values of the 7-story building were 5% lower than the 4-story building for all acceleration-related parameters. It was observed that the results obtained for the parameters in the other velocity and displacement groups were close to each other.
- It can be stated that the parameters in the velocity (except V_{rms} and SED) and acceleration groups are more dominant than the ones in the frequency and displacement groups because they have better correlations. On the other hand, it should be noted that both frequency and displacement-related parameters have low correlation values. Acceleration-related parameters have better correlation performance for short-period structures, e.g., 4-story models, whereas velocity-related parameters are best for medium-period systems such as 7-story buildings. This trend can be explained by the higher acceleration and velocity spectral ordinates in these period ranges, respectively.
- Among the acceleration-related parameters, I_a, I_c, A_{rms}, and SMA have the strongest correlation, while VSI, HI, and CAV show the best correlation in the velocity group. The correlation coefficients of these parameters are greater than 0.70. The good correlation of the above-mentioned parameters can be attributed to the cumulative calculation of these parameters and the energy demand.
- I_a has the best correlation and the lowest scatter with energy demands for acceleration group parameters; this result suggests that it is the best parameter to reflect the damage potential of earthquakes. Similar results were also reported by Cao and Ronagh (2014), Ozmen and Inel (2016), and Yang et al. (2009).
- VSI is also a good indicator of intensity measure and reflection of the potential damage. This consequence is also consistent with the studies carried out by Yakut and Yilmaz (2008), Kostinakis et al. (2015), Massumi and Gholami (2016), and Kamal and Inel (2021).
- As well-known parameters, PGA and PGV show a moderate correlation. This is also a parallel inference with Riddell and Garcia (2001), and Riddell (2007). It is estimated that the degree of correlation decreases because these parameters are obtained instantly as a single value, unlike the calculation of energy data.
- In the present study, the T_m, V_{max}/A_{max}, PGD, and D_{rms} parameters do not appear to be useful indicators of damage alone. The lowest correlations of these parameters have been emphasized by Cao and Ronagh (2014), and Ozmen and Inel (2016). Since considered buildings are not highly flexible systems, their periods do not have long periods. For this reason, it can be said that the performance of the parameters related to displacement (PGD and D_{rms}) is poor.

- This paper also investigated if the combination of multiple ground motion parameters by using multiple regression to reflect damage potential is better than a single parameter. Making use of the equations proposed for SDOF and MDOF systems via multiple regression, the correlation coefficients are increased to 0.945 and 0.937 with an increase of 5 and 10%, respectively.
- In addition to damage measures such as various damage indexes, interstory and roof drift ratios, it is concluded that input energy as highlighted in previous studies can also be used according to the findings in the present study.
- Even though the best parameters in studies where displacement is used as a damage indicator are velocity-related parameters, it was observed that both acceleration- and velocity-related parameters show good performance in this study. Since researchers calculate seismic loads by using the acceleration response spectrum for the design of new structures and strengthening of existing structures, it is recommended to use especially acceleration-related parameters for the prediction of seismic performance due to their familiarity with acceleration. In addition, it is thought that increasing the number of different types of parameters that show good correlation will enrich the diversity of future studies on the assessment of seismic hazard.

In order to obtain better correlation results, demands such as displacement and energy should be estimated accurately. For this reason, modeling of structures must be conducted properly. The period of buildings constructed in the regions like short, intermediate, and long periods also affects the behavior of the structure against earthquakes. Especially in the long period region, the stability of the spectral accelerations in the response spectrum of the earthquakes ensures that the demands of the structures in this region are close to each other. This can increase the correlation of their demands with considered the earthquake parameters. The choice of variables such as displacement and energy as demand measures affects the degree of correlation. Different variables (e.g. acceleration, velocity, displacement, and frequency) used in the calculation of ground motion parameters may be decisive in the correlation success. In addition, the relationship between parameters and demands is also influenced by the usage of regression types such as linear or nonlinear regression.

Declarations

Conflict of interest Author has no conflict of interest with others and third parties for the present manuscript.

References

Akkar S, Özen Ö (2005) Effect of peak ground velocity on deformation demands for SDOF systems. Earthq Eng Struct Dyn 34:1551–1571. https://doi.org/10.1002/eqe.492

Arias A (1970) Measure of earthquake intensity. Massachusetts Inst of Tech, Cambridge Univ of Chile, Santiago de Chile. pp 438–483

ASCE 41-13 (2014) Seismic evaluation and retrofit of existing buildings. American Society of Civil Engineers, USA

ATC-40 (1996) Applied technology council, seismic evaluation and retrofit of concrete buildings. California Seismic Safety Commission; California, USA

Baker JW (2007) Quantitative classification of near-fault ground motions using wavelet analysis. Bull Seismol Soc Am 97(5):1486–1501. https://doi.org/10.1785/0120060255

Benavent-Climent A, López-Almansa F, Bravo-González DA (2010) Design energy input spectra for moderate-to-high seismicity regions based on Colombian earthquakes. Soil Dyn Earthq Eng 30:1129–1148. https://doi.org/10.1016/j.soildyn.2010.04.022

Cabañas L, Benito B, Herraiz M (1997) An approach to the measurement of the potential structural damage of earthquake ground motions. Earthq Eng Struct Dyn 26:79–92

Cao V Van, Ronagh HR (2014) Correlation between seismic parameters of far-fault motions and damage indices of low-rise reinforced concrete frames. Soil Dyn Earthq Eng 66:102–112. https://doi.org/10.1016/j.soildyn.2014.06.020

Dindar AA, Yalçın C, Yüksel E, Özkaynak H, Büyüköztürk O (2015) Development of earthquake energy demand spectra. Earthq Spectra 31:1667–1689. https://doi.org/10.1193/011212EQS010M

Elenas A (1997) Interdependency between seismic acceleration parameters and the behaviour of structures. Soil Dyn Earthq Eng 16:317–322. https://doi.org/10.1016/S0267-7261(97)00005-5

Elenas A (2000) Correlation between seismic acceleration parameters and overall structural damage indices of buildings. Soil Dyn Earthq Eng 20:93–100. https://doi.org/10.1016/S0267-7261(00)00041-5

Elenas A, Meskouris K (2001) Correlation study between seismic acceleration parameters and damage indices of structures. Eng Struct 23:698–704. https://doi.org/10.1016/S0141-0296(00)00074-2

Fabrizio M, Bruno S, Decanini L, Saragoni R (2011) Correlations between energy and displacement demands for performance-based seismic engineering. Pure Appl Geophys 168:237–259. https://doi.org/10.1007/s00024-010-0118-9

Fahjan YM (2008) Selection and scaling of real earthquake accelerograms to fit the Turkish design spectra. Tech J Turkish Chamb Civ Eng 19:4423–4444

Fajfar P, Vidic T (1994) Consistent inelastic design spectra: hysteretic and input energy. Earthq Eng Struct Dyn 23:523–537. https://doi.org/10.1002/eqe.4290230505

FEMA-356 (2000) Federal emergency management agency, prestandard and commentary for the seismic rehabilitation of buildings. American Society of Civil Engineers (ASCE), Washington

Hori N, Inoue N (2002) Damaging properties of ground motions and prediction of maximum response of structures based on momentary energy response. Earthq Eng Struct Dyn 31:1657–1679. https://doi.org/10.1002/eqe.183

Housner GW (1952) Spectrum intensities of strong-motion earthquakes. Symp Earthq Blast Eff Struct. pp 20–36

Kamal M, Inel M (2021) Correlation between ground motion parameters and displacement demands of mid-rise rc buildings on soft soils considering soil-structure-interaction. Buildings 11(3):125. https://doi.org/10.3390/buildings11030125

Khashaee P, Mohraz B, Sadek F, Lew HS, Gross JL (2003) Distribution of earthquake input energy in structures. National Institute of Standards and Technology, Gaithersburg

Koç G (2017) Effects of ground motion characteristics on structural energy response of buildings. MSc Thesis, Istanbul Technical University

Kostinakis K, Athanatopoulou A, Morfidis K (2015) Correlation between ground motion intensity measures and seismic damage of 3D R/C buildings. Eng Struct 82:151–167. https://doi.org/10.1016/j.engstruct.2014.10.035

Kramer SL (1996) Geotechnical earthquake engineering. Prentice- Hall, Upper Saddle River

Liao WI, Loh CH, Wan S (2001) Earthquake responses of RC moment frames subjected to near-fault ground motions. Struct Des Tall Build 10:219–229. https://doi.org/10.1002/tal.178

Mander JB, Priestley MJN, Park R (1988) Theoretical stress-strain model for confined concrete. J Struct Eng 114:1804–1826. https://doi.org/10.1061/(asce)0733-9445(1988)114:8(1804)

Massumi A, Gholami F (2016) The influence of seismic intensity parameters on structural damage of RC buildings using principal components analysis. Appl Math Model 40:2161–2176. https://doi.org/10.1016/j.apm.2015.09.043

Merter O (2019) An investigation on the maximum earthquake input energy for elastic SDOF systems. Earthq Struct 16:487–499. https://doi.org/10.12989/eas.2019.16.4.487

Nuttli OW (1979) The relation of sustained maximum ground acceleration and velocity to earthquake intensity and magnitude. Miscellaneous Paper S-73-1 (Report 16), US Army Engineer Waterways Experiment Station, Vicksburg Mississippi

Okur A, Erberik MA (2014) Adaptation of energy principles in seismic design of Turkish RC frame structures. Part II: distribution of hysteretic energy. In: 15th world conference on earthquake engineering (15WCEE). Istanbul. pp 1–11

Ozmen HB, Inel M (2016) Damage potential of earthquake records for RC building stock. Earthq Struct 10:1315–1330. https://doi.org/10.12989/eas.2016.10.6.1315

Palanci M, Senel SM (2019) Correlation of earthquake intensity measures and spectral displacement demands in building type structures. Soil Dyn Earthq Eng 121:306–326. https://doi.org/10.1016/j.soildyn.2019.03.023

Papasotiriou A, Athanatopoulou A (2022) Seismic intensity measures optimized for low-rise reinforced concrete frame structures. J Earthq Eng 26(14):7587–7625. https://doi.org/10.1080/13632469.2021.1964650

Papasotiriou A, Athanatopoulou A, Kostinakis K (2022) Spectral acceleration as an efficient seismic damage measure for bare and masonry infilled R/C frames. J Earthq Eng 26(9):4580–4612. https://doi.org/10.1080/13632469.2020.1835751

PEER (2019) Pacific Earthquake Engineering Research Center; Berkeley University, California, USA. https://ngawest2.berkeley.edu/

Rathje EM, Abrahamson NA, Bray JD (1998) Simplified frequency content estimates of earthquake ground motions. J Geotech Geoenviron Eng 124:150–159

Reed JW, Anderson N, Chokshi NC, Kennedy RP, Metevia WJ, Ostrom DK, Stevenson JD (1988) A criterion for determining exceedance of the operating basis earthquake: final report

Riddell R (2007) On ground motion intensity indices. Earthq Spectra 23:147–173. https://doi.org/10.1193/1.2424748

Riddell R, Garcia JE (2001) Hysteretic energy spectrum and damage control. Earthq Eng Struct Dyn 30:1791–1816. https://doi.org/10.1002/eqe.93

SAP2000 (2018) Integrated finite element analysis and design of structures basic analysis reference manual. Computers and Structures Inc, Berkeley

Sarma SK, Yang KS (1987) An evaluation of strong motion records and a new parameter A95. Earthq Eng Struct Dyn 15:119–132. https://doi.org/10.1002/eqe.4290150109

SeismoSignal (2022) A computer program for processing of strong-motion data. Earthquake Engineering Solutions. https://seismosoft.com

Sucuoğlu H, Nurtuğ A (1995) Earthquake ground motion characteristics and seismic energy dissipation. Earthq Eng Struct Dyn 24:1195–1213. https://doi.org/10.1002/eqe.4290240903

Sucuoğlu H, Yücemen S, Gezer A, Erberik A (1998) Statistical evaluation of the damage potential of earthquake ground motions. Struct Saf 20:357–378. https://doi.org/10.1016/S0167-4730(98)00018-6

TBEC 2018 (2018) Turkish building earthquake code. Republic of Turkey Ministry of Interior Disaster and Emergency Management Presidency: Ankara, Turkey

Travasarou T, Bray JD, Abrahamson NA (2003) Empirical attenuation relationship for Arias Intensity. Earthq Eng Struct Dyn 32:1133–1155. https://doi.org/10.1002/eqe.270

Von Thun JL, Roehm LH, Scott GA, Wilson JA (1988) Earthquake ground motions for design and analysis of dams. Geotechnical special publication 20:463–481

Yakut A, Yilmaz H (2008) Correlation of deformation demands with ground motion intensity. J Struct Eng 134:1818–1828. https://doi.org/10.1061/(asce)0733-9445(2008)134:12(1818)

Yang D, Pan J, Li G (2009) Non-structure-specific intensity measure parameters and characteristic period of near-fault ground motions. Earthq Eng Struct Dyn 38:1257–1280. https://doi.org/10.1002/eqe.889

Ye L, Otani S (1999) Maximum seismic displacement of inelastic systems based on energy concept. Earthq Eng Struct Dyn 1499:1483–1499

Zhai C, Chang Z, Li S, Chen Z, Xie L (2013) Quantitative identification of near-fault pulse-like ground motions based on energy. Bull Seismol Soc Am 103(5):2591–2603. https://doi.org/10.1785/0120120320

Zhu TJ, Tso WK, Heidebrecht AC (1988) Effect of peak ground a/v ratio on structural damage. J Struct Eng 114:1019–1037. https://doi.org/10.1061/(asce)0733-9445(1988)114:5(1019)